Phylogenetic relationship of a fossil macaque (*Macaca* cf. *robusta*) from the Korean Peninsula to extant species of macaques based on zygomaxillary morphology

Tsuyoshi Ito[1], Yung-jo Lee[2], Takeshi D. Nishimura[1], Mikiko Tanaka[1], Jong-yoon Woo[2], Masanaru Takai[1]

[1]Department of Evolution and Phylogeny, Primate Research Institute, Kyoto University, Inuyama, Aichi 484-8506, Japan

[2]Institute of Korean Prehistory, 2559, Yongam-dong, Sangdang-gu, Cheongju, Chungbuk 28763, Korea

* Corresponding author: Tsuyoshi Ito

Telephone: +81-568-63-0523, Fax: +81-568-61-5775

E-mail: ito.tsuyoshi.3a@kyoto-u.ac.jp

Keywords: Biogeography; Computed tomography; East Asia; *Macaca*; Phylogentic morphometrics

Abstract

Little is known about the biogeographical and evolutionary histories of macaques (*Macaca* spp.) in East Asia because the phylogenetic positions of fossil species remain unclear. Here we examined the zygomaxillary remains of a fossil macaque (*M.* cf. *robusta*) from the Durubong Cave Complex, South Korea, that dates back to the late Middle to Late Pleistocene, to infer its phylogenetic relationship to extant species. We took 195 fixed- and semi-landmarks from the zygomaxillary regions of the fossil specimen and from 147 specimens belonging to 14 extant species. We then conducted a generalized Procrustes analysis followed by a multivariate statistical analysis to evaluate the phenetic affinities of the fossil to the extant species and reconstructed the most parsimonious phylogenetic tree using a phylogenetic morphometric approach. We found that the fossil was most similar to

M. fuscata (Japanese macaque) in the zygomaxillary morphospace although it was at the limit of the range of variation for this species. The second closest in the morphospace was the continental *M. mulatta* (rhesus macaque). Parsimonious reconstruction confirmed that the fossil was most closely related to *M. fuscata*, even after controlling for the effects of allometry. These findings suggest that in the late Middle to Late Pleistocene, close relatives of *M. fuscata* that looked like the extant species were distributed on the Korean Peninsula, where no species of macaques are found today. Thus, some morphological characteristics of *M. fuscata* may have developed before its ancestor dispersed into the Japanese archipelago.

1. Introduction

The genus *Macaca* consists of approximately 20 extant species and occupies a wider range of climates and habitats than any other genus of nonhuman primates (Fleagle, 2013). Consequently, macaques have attracted much attention as an analogy to understand how humans left tropical regions and adapted to various other environments (Rae et al., 2003; Márquez and Laitman, 2008; Hanya et al., 2011; Karen J, 2011; Tsuji et al., 2013; Ito et al., 2015). Furthermore, some East Asian species, particularly *M. mulatta* (rhesus macaque) and *M. fuscata* (Japanese macaque or snow monkey), are often used in biological laboratory

47 studies (Sibal and Samson, 2001). To better understand these cold-adapted and well-studied
48 species, we need to understand their biogeographic and evolutionary histories, particularly at
49 the northern limit of their distribution in East Asia.

50 The phylogeny of extant species of macaques has been well studied, with most molecular
51 phylogenetic studies (Tosi et al., 2000; Li et al., 2009; Jiang et al., 2016), except
52 mitochondrial studies (Morales and Melnick, 1998; Liedigk et al., 2014), supporting the
53 classification of Delson (1980). Delson's classification subdivides macaques into four
54 phylogenetic groups: *fascicularis*, *sinica*, *silenus*, and *sylvanus* groups. A molecular
55 phylogenetic study by Jiang et al. (2016) suggested that the African *sylvanus* group first
56 diverged ca. 5.5 million years ago (Mya), the *silenus* group diverged ca. 4.5 Mya, and the
57 *fascicularis* and *sinica* groups diverged ca. 3.5 Mya.

58 The most recently diverged groups (i.e., *fascicularis* and *sinica* groups) are distributed
59 in East Asia and partly overlap each other (Fooden, 1988, 2006). The *fascicularis* group
60 consists of four extant species, including *M. fuscata* and *M. mulatta*, which are found in
61 temperate regions: *M. fuscata* is distributed in the Japanese archipelago, which is at the
62 northernmost limit of extant nonhuman primates (Fooden and Aimi, 2005), while *M. mulatta*
63 is widely distributed from Afghanistan to southern China (Fooden, 2000). The *sinica* group

64 consists of at least five (Sinha et al., 2005; possibly six or seven; Chakraborty et al., 2007; Li
65 et al., 2015; Fan et al., 2016) extant species, with some of the large-bodied species, such as
66 *M. thibetana*, *M. assamensis*, and *M. leucogenys*, distributed in high-altitude areas in southern
67 China (Fooden, 1982, 1983; Li et al., 2015). Thus, both phylogenetic groups inhabit relatively
68 cold environments in East Asia. However, no species currently inhabit northern China and
69 the Korean Peninsula, isolating *M. fuscata* from the other continental species.

70 However, some excavations of Pleistocene fossil macaques have been reported from
71 northern China and the Korean Peninsula (Schlosser, 1924; Young, 1934; Zhang et al., 1986;
72 Pan and Jablonski, 1987; Park and Lee, 1998; Takai et al., 2008). The first record of a fossil
73 macaque from East Asia was *M. anderssoni*, which was described from a nearly complete
74 face excavated from the Early Pleistocene sediment of Mianchi, Henan Province, China
75 (Schlosser, 1924). A decade later, another species, *M. robusta*, was described from a partial
76 maxilla excavated from the Middle Pleistocene sediment of Choukoutien, Beijing, China
77 (Young, 1934). Since then, nearly all of the fossil specimens that have been discovered in
78 northern China or the Korean Peninsula from the Early to Middle Pleistocene have been
79 referred to as one of these two fossil species. Although *M. anderssoni* has a larger dental size
80 than *M. robusta*, it is sometimes considered a junior synonym of the latter (Simons, 1970;

81 Delson, 1980; but see Fooden, 1990). These fossils are believed to fill the biogeographical
82 gap in the current distribution of macaques, which will potentially elucidate their evolutionary
83 histories. However, the phylogenetic relationships of these fossils and extant species remain
84 controversial (Delson, 1977, 1980; Jablonski and Pan, 1988; Fooden, 1990; Pan and
85 Yanzhang, 1995; Park and Lee, 1998; Ito et al., 2014b), particularly with regard to whether
86 they are phylogenetically related to members of the *sinica* group or the *fascicularis* group.

87 The fossil records from the Korean Peninsula is key to understanding the evolution of
88 *M. fuscata* in particular. Some fossil macaques have been reported from the Middle and Late
89 Pleistocene sediments of several localities in the Korean Peninsula (Park and Lee, 1998;
90 Fooden and Aimi, 2005; Lee and Woo, 2005; Lee, 2006; Lee and Takai, 2012; Lee et al.,
91 2013). Most of these fossils are isolated teeth or partial fragments of skeletons, but the fossil
92 specimen excavated by the Chungbuk National University Museum Team from the Durubong
93 (=Turupong) Cave Complex, Cheongju City, Chungbuk Province, South Korea, is a well-
94 preserved zygomaxillary region (Fig. 1). This was identified as *M.* cf. *robusta* by Park and
95 Lee (1998), who reported that its morphology was intermediate between *M. robusta* and *M.*
96 *fuscata* but more similar to *M. robusta* with regard to tooth size. Lee and Takai (2012) stated
97 that the upper molars of the Korean fossils were relatively large, making them comparable

98 with those of *M. anderssoni*, while the lower molars were relatively small compared with
99 other fossil and extant macaques. Furthermore, they also stated that most of the Korean fossils
100 retain some accessory cusps (distoconules, interconulus, 6th cusp, and 7th cusp), which are
101 frequently found in the molars of *M. fuscata* (Lee and Takai, 2012). Fooden and Aimi (2005)
102 demonstrated that measurements of the Korean fossil molars were within the range of
103 variation shown by *M. fuscata*. Together, these findings imply that the Korean fossils may be
104 related to the ancestors of *M. fuscata* or the other fossil species, namely *M. anderssoni* and/or
105 *M. robusta*; and that more than one lineage may have been distributed in the Korean Peninsula
106 during the Middle to Late Pleistocene. However, most previous studies have based their
107 conclusions on tooth morphology alone, and no phylogenetic assessment of the fossil species
108 in comparison with the various extant species of macaques has been conducted to date.

109 In this study, we compared the morphology of the zygomaxillary region in the Korean
110 fossil specimen that was discovered in the Durubong Cave Complex with that of extant
111 species of macaques. This is the most well-preserved fossil macaque specimen in Korea.
112 Zygomaxillary morphology is likely to be informative for the reconstruction of phylogenetic
113 relationships, because zygomaxillary shape can be partially differentiated among the four
114 phylogenetic groups in macaques (Ito et al., 2014a) and has some phylogenetic signal (Ito et

115 al., 2014a). First, we evaluated the pattern of zygomaxillary variation in extant species and
116 estimated the evolutionary and phylogenetic significance of this variation. We then assigned
117 the fossil to the morphospace of the extant species and performed a cladistic analysis to infer
118 the evolutionary and phylogenetic relationships of this fossil to the extant species. To do this,
119 we used semi-landmark-based geometric morphometrics to capture the surface topography
120 of the zygomaxillary region, because anatomically defined landmarks were limited on the
121 fossil. Moreover, we examined the nasal cavity morphology using computed tomography
122 (CT), because it has been reported that this reflects phylogenetic relationships (Ito et al.,
123 2014b; Nishimura et al., 2014; Ito and Nishimura, 2016). Based on the findings of these
124 analyses, we discuss the biogeographic and evolutionary histories of East Asian macaques.

125 **2. Materials and methods**

126 *2.1. Molecular phylogeny*

127 The phylogeny that was used for the phylogenetic comparative analyses was estimated
128 using 11 mitochondrial and 53 nuclear DNA sequences (Supplementary Online Material
129 [SOM] Table S1). The DNA sequences were obtained from the 10KTrees webserver (Arnold
130 et al., 2010; http://10ktrees.fas.harvard.edu/Primates/) and Perelman et al. (2011). The

131 sequences were aligned using MAFFT version 7 (Katoh and Standley, 2013) and then
132 concatenated using SequenceMatrix software (http://gaurav.github.io/taxondna/). BEAST 2
133 software (Bouckaert et al., 2014) was used for phylogenetic inference using a site model that
134 was estimated by the Bayesian approach with the bModelTest package (Bouckaert, 2015).
135 Markov Chain Monte Carlo simulations were performed for 10,000,000,000 generations with
136 a sampling frequency of 100,000. Five species belonging to the subtribe Papionina
137 (*Cercocebus torquatus*, *Lophocebus aterrimus*, *Mandrillus sphinx*, *Papio hamadryas*, and
138 *Theropithecus gelada*) were used as an outgroup. The maximum clade credibility tree was
139 chosen after removing a 10% burn-in using TreeAnnotator version 2.4.7 (SOM Fig. S1).

140 *2.2. Cranial sample*

141 For the fossil specimen, we used the zygomaxillary specimen of a fossil macaque stored
142 at the Chungbuk Natural History Museum, Chungbuk, South Korea (2ㅜㄷ-12-2169; Fig. 1),
143 which has been partially broken and repaired. The fully erupted third molars and relatively
144 large canines indicate that this individual was an adult male. This specimen originated from
145 the Durubong (=Turupong) Cave Complex, Cheongju City, Chungbuk Province, South Korea.
146 The faunal composition of Durubong Cave Complex (*Ursus arctosi*, *Crocuta ultima*,
147 *Dicerorhinus* cf. *choukoutiensis*, and *M.* cf. *robusta*) suggests that this specimen dates back

148 to the late Middle Pleistocene to the Late Pleistocene period (Park and Lee, 1998), while the
149 faunal complex together with the results of pollen analyses suggests that this was a warm
150 (interglacial or interstadial) period (Lee and Woo, 2005).

151 For the extant samples, we used the dry crania with almost-erupted or fully erupted third
152 molars from 147 adult males belonging to 14 extant species (Table 1). These specimens are
153 stored at eight institutes in Japan and USA, which are listed in SOM Table S2. Sulawesi
154 macaques were not included in the sample because of their unusual cranial morphology
155 (Albrecht, 1978). The samples consisted of wild (n = 80), captive (n = 35), and unknown-
156 origin specimens (n = 32), but any pathological specimens, which showed evidence of severe
157 alveolar pyorrhea and/or unusual deflection of muzzles, were not included in the samples.
158 ANOVA showed that the differences in zygomaxillary shape among wild, captive, and
159 unknown-origin specimens were significant in some cases, but were much smaller compared
160 with interspecies differences (SOM Table S3).

161 *2.3. CT examinations*

162 CT images were acquired for the fossil specimen and 134 specimens of extant species.
163 The zygomaxillary fragment of the Korean fossil specimen (2ㅜㄷ-12-2169) was scanned

164 using a helical scanner (HiSpeed; GE Medical Systems Inc., Waukesha, WI, USA) at the
165 veterinary medical center of Chungbuk National University, Chungbuk, South Korea, with a
166 pixel size of 0.1 mm and a slice thickness of 1.0 mm. The original volume data were then
167 reconstructed to give a slice thickness of 0.3 mm. CT scans of the extant species were
168 obtained previously (Ito and Nishimura, 2016) and are available at the Digital Morphology
169 Museum, Kyoto University (http://dmm.pri.kyoto-u.ac.jp), with the exception of specimens
170 that were not permitted for release due to copyright restrictions (SOM Table S2), or from
171 MorphoSource (http://www.morphosource.org).

172 The internal structure of the maxilla was observed using Amira 5.5. In particular, we
173 investigated the degree of lateral expansion of the nasal cavity and the maxillary thickness,
174 which are considered to reflect phylogenetic relationships in macaques (Ito et al., 2014b).

175 *2.4. Geometric morphometrics*

176 Three-dimensional (3D) surface models of the face were obtained from the Smithsonian
177 3D collection of primates (http://humanorigins.si.edu/evidence/3d-collection/primate) or
178 constructed from the serial CT images using Amira 5.5 software (FEI Visualization Sciences
179 Group, Bordeaux, France). Details of the 3D surface modeling were described in a previous

paper (Ito and Nishimura, 2016). Small superficial holes, if any, were manually filled using Amira 5.5 or Rapidform XOS3 64. Where the left side of the face was broken, the 3D surface model was horizontally flipped using MeshLab software (http://www.meshlab.net). Because the repair of the fossil specimen was slightly imperfect (i.e., the joins of fragments were not smooth; Fig. 1), we slightly re-repaired the fossil specimen virtually using Amira 5.5 software so that the joins of fragments were smooth and the repaired specimen had a more natural appearance (Fig. 2).

In total, 195 landmarks were taken on the 3D surface models (left side of the face) using Stratovan Checkpoint software (Stratovan Corporation, Sacramento, CA, USA; Fig. 3). This included 22 anatomically defined landmarks, 42 semi-landmarks on curves, and 131 semi-landmarks on the surface (SOM Table S4). Missing landmarks (16 landmarks in nine specimens) were estimated by deforming the configurations of the weighted average of the complete dataset for the same species using a thin-plate spline (TPS) interpolation calculated from the available landmarks. The semi-landmarks were slid on curves or surfaces so that the bending energy of TPS deformation was minimal (Gunz et al., 2005). These procedures were performed using the package "Morpho" version 2.5.1 (Schlager, 2017) in R software version 3.4.1 (R Core Team, 2017). Following sliding, the semi-landmarks were treated in the same

197 way as the homologous landmarks in subsequent analyses.

198 All of the final coordinates were subjected to generalized Procrustes analysis (GPA),
199 which registered the landmark configurations across all individuals to produce Procrustes
200 coordinates. The centroid size was simultaneously calculated as the square root of the sum of
201 the square distances of all landmarks from their centroid. To evaluate non-allometric
202 variations, we also produced size-adjusted shape components by calculating the residuals of
203 the multiple regression of Procrustes coordinates on natural-logarithmically transformed
204 centroid size (lnCS) using MorphoJ version 1.06d (Klingenberg, 2011), wherein 16.2% of
205 the shape variance was explained by lnCS ($p < 0.0001$).

206 We then calculated species mean values. To do this, GPA was conducted for each
207 species, and the mean shapes of the 15 operational taxonomic units (the 14 extant species and
208 the fossil specimen) were then subjected to another GPA. A size-adjusted shape component
209 was then calculated in the same way as mentioned above but on a species mean basis, wherein
210 27.2% of the shape variance was explained by lnCS ($p = 0.0012$).

211 The individual values were used in the phenetic analyses, while the species mean values
212 were used in the phylogenetic comparative and cladistic analyses. Each of these analyses was

213 conducted twice using the raw and size-adjusted shape data.

214 *2.5. Phenetic analyses*

215 The phenetic affinity of the fossil specimen was evaluated to assign it to the
216 morphospace of the extant species. To detect shape vectors that exhibited interspecies
217 differences, between-group principal component analyses (bgPCAs) were performed. The
218 bgPCA is the projection of data onto the principal components of the group means
219 (Mitteroecker and Bookstein, 2011). In this study, the species means for extant species were
220 included in the calculation of the covariance matrix, following which the individuals of extant
221 species and the fossil specimens were projected onto the bgPCA axes. This step was
222 performed using the "plotTangentSpace" function of the "geomorph" package with some
223 modifications. Shape changes along the bgPC axes were visualized using R, Amira 5.5, and
224 Rapidform XOS3 64.

225 Procrustes distances were calculated from the fossil specimen to all extant individuals
226 to quantify its phenetic affinity to extant species using the R package "shapes" version 1.2.0
227 (Dryden, 2016).

2.6. Phylogenetic comparative analyses

Phylogenetic comparative analyses were performed to evaluate the phylogenetic significance and evolutionary polarity of zygomaxillary shape. A phylomorphospace (Sidlauskas, 2008) was obtained to reconstruct the evolutionary changes in zygomaxillary shape along the tree using the "plotGMPhyloMorphoSpace" function of the "geomorph" package with some modifications. A phylomorphospace is a PCA of the species mean values and the inferred ancestral shapes, with the phylogeny mapped onto the plane of the PCs. This was produced using only the extant species (and the inferred ancestral nodes), following which the fossil specimen was extrapolated into the PC axes. The phylogenetic signal in zygomaxillary shape was evaluated using the "physignal" function of the "geomorph" package. The significance of the phylogenetic signal was then tested using permutation procedures with 9,999 iterations.

2.7. Cladistic analyses

A phylogenetic morphometric approach (Catalano et al., 2010; Goloboff and Catalano, 2011) was used to estimate the phylogenetic relationship between the fossil specimen and the extant species examined. This approach parsimoniously detects the ancestral points that

minimize the distance between the ancestor and descendant points along the tree and has been shown to have a better performance than other landmark-based cladistic approaches (Catalano and Torres, 2016). We performed the cladistic analyses using the species mean values of the Procrustes coordinates with the Windows GUI version of TNT 1.5 software (Goloboff et al., 2008; Goloboff and Catalano, 2016), setting *M. sylvanus* as an outgroup and searching for the best tree with and without monophyly constraints. Considering previous molecular phylogenetic studies of Alu elements (Li et al., 2009; Jiang et al., 2016), the constraints were forced as follows: [([arc, ass, thi], [rad, sin]), ([fus, mul, cyc], fas)], (leo, sil, sib, nem); the fossil was allowed to move freely (for abbreviations, see Table 1). Landmark optimization was set as six grid cells and one nesting with iterations. A traditional search was conducted, which consisted of Wagner trees with 10 replications followed by tree bisection reconnection. Resampling was performed to evaluate phylogenetic uncertainty, wherein symmetric resampling with 33% change probability was conducted, and the frequency difference (GC values; Goloboff, 2003) was calculated.

3. Results

3.1. Internal structures

The internal structures of the maxilla in the extant species are shown in Figure 4. The large-bodied species of the *sinica* group, namely *M. arctoides*, *M. assamensis*, and *M. thibetana*, often exhibited a laterally expanded nasal cavity with thin maxillary walls, which was well represented at the M^1 level (this corresponds approximately to the level at which the nasal cavity shows a maximum width). By contrast, other species, including members of the *fascicularis*, *silenus*, and *sylvanus* groups, usually had limited lateral expansion of the nasal cavity and a relatively thick maxillary wall.

In the fossil specimen, the lateral and upper walls of the nasal cavity were broken (Fig. 5). Nevertheless, based on the surrounding structures, it appeared that the nasal cavity was not as greatly expanded laterally as those of the large-bodied species of the *sinica* group, and the maxillary walls were relatively thick.

3.2. Phenetic affinities of zygomaxillary shape

The bgPCA for the raw shape data showed allometric and non-allometric variations in the zygomaxillary shape (Fig. 6). bgPC1 and bgPC2 accounted for 47.2% and 18.0% of the

274 total interspecies variance, respectively; bgPC1 was positively correlated with lnCS ($r = 0.70$,
275 $p < 0.001$), whereas bgPC2 was not ($r = 0.10$, $p = 0.238$). Individuals with more positive
276 bgPC1 scores (and thus larger lnCS) tended to have muzzles that were longer, superior-
277 inferiorly shorter, and narrower, had a more prominent canine alveolus, and were more
278 ventrally oriented at the anterior portion (Fig. 7). The intercept of this allometric trajectory
279 was significantly different among the species groups (ANCOVA, $p = 0.010$; the *sylvanus*
280 group was excluded from this analysis due to its small sample size), but their distributions
281 highly overlapped each other. Individuals with more positive bgPC2 scores tended to have
282 less prognathic and higher muzzles, with a wider posterior portion compared with the anterior
283 portion. The *fascicularis* and *sylvanus* groups had high bgPC2 scores compared with the other
284 two groups, although their distributions also considerably overlapped.

285 The bgPCA for the size-adjusted shape data exhibited non-allometric variations (Fig. 6),
286 with bgPC1 and bgPC2 accounting for 27.2% and 16.4% of this interspecies variance,
287 respectively. In contrast to the bgPCA for the raw shape data, bgPCA for the size-adjusted
288 shape data did not show a variation in facial elongation (Fig. 7). A more positive bgPC1 score
289 was associated with a more inferior deflection of the anterior portion of the muzzle against
290 the posterior portion. The shape changes, as well as interspecies group differences along the

291 bgPC2 axis, were almost identical to those shown for bgPC2 of the raw shape data, but in the
292 opposite direction.

293 For the fossil specimen, lnCS and bgPC1 were approximately intermediate among the
294 macaques (Fig. 6). The bgPC2 showed that the fossil specimen had a less prognathic and
295 higher muzzle, and the posterior portion of the muzzle was wider than the anterior portion,
296 making it similar to members of the *fascicularis* and *sylvanus* groups. In particular, the fossil
297 specimen was closest to or within the ranges of variation for *M. fuscata* and *M. mulatta*, as
298 seen in the scatterplots of lnCS and bgPC scores. Figure 8 shows the Procrustes distances
299 from the fossil specimen to each of the examined individuals of extant species. For both the
300 raw and size-adjusted shape data, the fossil specimen was the most similar to *M. fuscata* and
301 the least similar to species of the *silenus* group. The other species were positioned
302 intermediate between these two extremes, but *M. thibetana* was similar to the fossil when
303 size was adjusted.

304 *3.3. Phylogenetic comparisons*

305 A moderate phylogenetic signal was detected in the raw shape data (K = 0.42, p =
306 0.0163) but was marginally significant in the size-adjusted shape data (K = 0.36, p = 0.0627).

307 The phylomorphospace demonstrated evolutionary changes in the zygomaxillary shape
308 (Fig. 9). For the raw shape data, PC1 and PC2 accounted for 50.4% and 17.5% of the variance,
309 respectively, and PC1 was positively correlated with lnCS (r = 0.79, p = 0.0009), whereas
310 PC2 was not (r = 0.06, p = 0.831). Shape changes along these PC axes showed similar patterns
311 to the bgPCA of the raw shape data (SOM Fig. S2). For the size-adjusted shape data, PC1
312 and PC2 accounted for 27.7% and 26.4% of the variance, respectively. More positive PC1
313 scores were associated with a more prominent canine alveolus and with the anterior portion
314 of the muzzles being deflected more inferiorly against the posterior portion. Shape changes
315 along PC2 were almost identical to those shown in the raw shape data, but in the opposite
316 direction.

317 The fossil specimen was positioned near the branch of *M. fuscata* for both the raw and
318 size-adjusted shape data (Fig. 9). The clade that included *M. fuscata*, *M. mulatta*, and *M.*
319 *cyclopis*, as well as *M. sylvanus*, deviated from the ancestral nodes in phylomorphospace.
320 Although the degree of deviation was limited compared with the two lineages, *M. thibetana*
321 also approached the derived fields of the phylomorphospace, particularly when size was
322 adjusted. Such deviations indicated that these lineages independently acquired similar derived
323 features (i.e., a less prognathic and higher muzzle, whose posterior portion was narrower than

the anterior portion).

3.4. Cladistic analyses

Cladistic analyses were performed based on the 3D landmark data from the zygomaxillary region (Fig. 10). The unconstrained models reconstructed trees whose topologies were quite different from the molecular phylogenetic trees (Li et al., 2009; SOM Fig. S1), indicating that there is some homoplasy in the zygomaxillary morphology. The best tree scores, which indicate the sum of the differences between the shapes of the ancestor and descendants for all tree branches (Goloboff and Catalano, 2016), were 3.21664 and 3.41040 for the raw and size-adjusted shape data, respectively. When the analyses were repeated with monophyly constraints, which searched for the most parsimonious scenario within the constraints, the best tree scores were 3.70956 and 3.85731 for the raw and size-adjusted shape data, respectively. In all four cases, the phylogenetic proximity between the fossil specimen and *M. fuscata* was supported.

4. Discussion

4.1. Patterns of zygomaxillary variation in extant species

We observed allometric variations in zygomaxillary shape among the extant species

340 examined. As commonly found in papionin crania (Singleton, 2002; Frost et al., 2003; Gilbert
341 and Grine, 2010; Ito et al., 2014a), we confirmed that larger individuals tended to have more
342 elongated and inferiorly deflected muzzles. Such allometric shape components should be
343 interpreted with care in phylogenetic studies because they can obscure phylogenetic signal.
344 For example, although bgPC1 showed that an elongated and inferiorly deflected muzzle is
345 characteristic of members of the *silenus* group, this feature is actually just a scaled-up version
346 of that found in small-bodied taxa. Similarly, the shape components that were represented by
347 PC1 of the phylomorphospace were also allometric and therefore problematic. Although
348 allometric shape components are potentially phylogenetically informative (Gilbert and Rossie,
349 2007; Gilbert et al., 2009), we were unable to detect clear differences in allometric vectors
350 among the four phylogenetic groups. Furthermore, although size itself may provide some
351 phylogenetic information, it is inappropriate to rely on a single trait (i.e., size) when inferring
352 phylogenetic relationships (see Pearson et al., 2015).

353 Non-allometric shape components were observed in two ways. First, bgPC2 and PC2 of
354 phylomorphospace based on the raw shape data were independent of size, which can be
355 interpreted as non-allometric. Second, the size-adjusted shape components, which were the
356 residuals of a multiple regression of raw Procrustes shape components on lnCS (Monteiro,

357 1999; Drake and Klingenberg, 2008; Klingenberg, 2011), were free from allometric
358 associations, although they had also partially lost some phylogenetic information in the
359 process (see Gilbert, 2011). These non-allometric shape components did not include facial
360 elongation but could be characterized by the degrees of height and prognathism of the muzzle,
361 as well as some localized shape changes in the zygomaxillary region.

362 The phylogenetic significance and evolutionary polarity of zygomaxillary shape were
363 evaluated. The phylomorphospace suggested that a higher and less prognathic muzzle was a
364 derived condition in macaques as shown in PC2, and this was observed in the clade that
365 includes *M. fuscata*, *M. mulatta*, and *M. cyclopis* of the *fascicularis* group, as well as *M.*
366 *thibetana* and *M. sylvanus*. These lineages all inhabit relatively cold environments, and
367 therefore this shape change may reflect parallel adaptive evolution to a cold environment,
368 although further testing is required to verify this hypothesis. The degree of change along this
369 PC2 axis, however, varies among lineages; *M. fuscata* is located at the extreme end of this
370 axis (and thus has the highest and least prognathic muzzle), followed by *M. sylvanus*, close
371 relatives of *M. fuscata* (*M. mulatta* and *M. cyclopis*), and *M. thibetana*. The difference in the
372 degree of the shape change among phylogenetic groups could be explained by phylogenetic
373 constraints, as suggested by the finding that some phylogenetic signal is detected in the

374 zygomaxillary shape, although it is marginally significant for size-adjusted shape data.

375 In addition, previous studies have indicated that variations in the nasal cavity can be
376 explained by phylogeny but not by allometry (Ito et al., 2014b; Ito and Nishimura, 2016).
377 Here, the most notable characteristics are a laterally expanded nasal cavity and thin lateral
378 maxillary walls at the anterior portion of the muzzle, which are often seen in the three large-
379 bodied species of the *sinica* group (*M. arctoides*, *M. assamensis*, and *M. thibetana*). These
380 internal features are considered to be derived traits in macaques (Ito et al., 2009; Ito et al.,
381 2014b). Certainly, nasal cavity morphology also varies in relation to ecological adaptation
382 and developmental plasticity. For example, in modern humans, individuals in colder
383 environments tend to have a narrower nasal cavity (Noback et al., 2011), while in Japanese
384 macaques, individuals in colder environments tend to have a larger cross-sectional area of the
385 cavity (Rae et al., 2003); such clinal variations are generally considered to be a consequence
386 of adaptation to climate. Additionally, cold environment-reared rats have smaller nasal
387 cavities than a corresponding control group, which reflects developmental plasticity (Rae et
388 al., 2006). Nevertheless, it is difficult to explain, solely by such environmental factors, why
389 an expanded nasal cavity is often found in the three-large-bodied species of the *sinica* group
390 but is barely observed in other cold environment-inhabiting species such as *M. sylvanus* and

391 *M. fuscata*. Therefore, the derived traits of internal structures that are found in members of
392 the *sinica* group as well as those of zygomaxillary shape that are typically found in members
393 of the *fascicularis* and *sylvanus* groups are considered to be informative for estimating the
394 phylogenetic relationships of a fossil specimen.

395 *4.2. Characteristics of the Korean fossil specimen and their phylogenetic significance*

396 The Korean fossil specimen was most similar to *M. fuscata* in several characteristics.
397 However, it must be remembered that a phenetic affinity does not necessarily reflect
398 phylogenetic relatedness. The nasal cavity of the Korean fossil specimen exhibited moderate
399 lateral expansion, making it similar to members of the *fascicularis* group and some of the
400 other groups. However, this is not considered to be a derived character (Ito et al., 2014b) and
401 so cannot be used to imply their phylogenetic relatedness. The Korean fossil specimen also
402 had a somewhat similar level of facial elongation to some other species, such as *M. fuscata*.
403 However, since this feature is largely associated with size, its reliability for phylogenetic
404 interpretation is also questionable. The long-standing controversies around the phylogenetic
405 relationships of fossil macaques (Delson, 1977, 1980; Jablonski and Pan, 1988; Fooden,
406 1990; Pan and Yanzhang, 1995; Park and Lee, 1998; Ito et al., 2014b) could be partly ascribed
407 to the use of such confusing characteristics.

408 The Korean fossil specimen has a vertically high and less prognathic muzzle, which is
409 the same as the clade that includes *M. mulatta*, *M. cyclopis*, and *M. fuscata*, as well as *M.*
410 *sylvanus*. This shape component is independent of allometry and is probably a derived
411 condition in macaques. It is not likely that the Korean fossil is closely related to the African
412 species *M. sylvanus*. Among the three species of the clade, the Korean fossil was most similar
413 to *M. fuscata*, followed by *M. mulatta*, with features that lay within the range of intraspecific
414 variation for each. Furthermore, cladistic analyses also confirmed phylogenetic relatedness
415 between the Korean fossil specimen and *M. fuscata*. Although *M. thibetana* is similar to the
416 Korean fossil, particularly for the size-adjusted shape data, the degree of similarity is limited
417 compared with *M. fuscata*. Therefore, it is reasonable to consider that the Korean fossil
418 specimen is phylogenetically related to the clade that includes *M. mulatta*, *M. cyclopis*, and
419 *M. fuscata,* particularly to *M. fuscata*.

420 It should be noted here that this finding does not necessarily suggest a phylogenetic
421 closeness between members of the *fascicularis* group and the Chinese fossil species, namely
422 *M. robusta* and *M. anderssoni*. Although the fossil macaques discovered from the Korean
423 Peninsula are sometimes referred to as *M. robusta* (Park and Lee, 1998; Lee and Woo, 2005),
424 some or all of them may be actually unrelated to this fossil species. Further studies are

425 expected to elucidate the phylogenetic relationships among the fossil specimens in East Asia.

426 *4.3. Biogeographical and evolutionary implications*

427 The present study suggests that the Korean fossil specimen is phylogenetically related
428 to the *fascicularis,* rather than the *sinica,* group of macaques. Delson (1980) and Ito et al.
429 (2014b) suggested that the proto-members of the *sinica* group, for example, *M. anderssoni*,
430 were largely distributed in northern China in the Early Pleistocene and that members of this
431 group may have retreated southward and been replaced by latecomers, that is, members of
432 the *fascicularis* group, likely by the Middle Pleistocene (Delson, 1980; Ito et al., 2014b). This
433 scenario is congruent with the present inference that the macaques living on the Korean
434 Peninsula in the late Middle to Late Pleistocene were related to the *fascicularis* group.

435 The late Middle to Late Pleistocene period is likely later than the divergence time
436 between *M. fuscata* and *M. mulatta*, which is considered to be ca. 0.4–1.4 Mya based on
437 molecular studies and fossil evidence from Japan (Fooden and Aimi, 2005; Fooden, 2006;
438 Chu et al., 2007; Jiang et al., 2016). Therefore, the Korean macaque is not the direct ancestor
439 of *M. fuscata* but rather belongs to a collateral line that diverged from the main line of *M.*
440 *fuscata*, *M. mulatta*, or the common ancestral lineage of the two species. They are probably

441 remnants that had been retained in the Korean Peninsula. Alternatively, the Korean macaque
442 may be a subpopulation of Japanese macaques that had returned from the Japanese
443 archipelago. In light of the parsimony principle, the former scenario is more probable. In
444 either case, the Korean lineage could have become extinct due to an inability to escape the
445 Korean Peninsula during the Late Pleistocene glacial period.

446 The zygomaxillary shape of the Korean fossil specimen is intermediate between *M.*
447 *fuscata* and *M. mulatta* but more similar to the former. It has previously been suggested that
448 the distinct morphological characteristics of *M. fuscata* developed after its dispersal into the
449 Japanese archipelago (Fooden, 2006). However, assuming that the Korean macaque is not the
450 lineage that has returned from the Japanese archipelago, it follows that the morphological
451 evolution of these features started before this dispersal. These findings fill in some of the
452 biogeographical and evolutionary gaps between *M. fuscata* and continental lineages,
453 potentially shedding light on cold adaptation in primates.

454 *4.4. Limitations of this study*

455 This study has several important limitations, particularly related to sample composition.
456 First, the sample size is small for both extant (n = 2–53/species) and fossil species (n = 1).

457 This limitation risks an underestimation of intraspecific variation and reduces the reliability
458 of species mean value estimation (Cardini and Elton, 2007; Schillaci and Schillaci, 2009).
459 Second, the sample includes not only wild-caught specimens but also captive and unknown-
460 origin specimens. We demonstrated that the morphological differences among specimen
461 sources were small compared with interspecies differences, but were significant in some cases.
462 Therefore, our interpretation of the results, which mainly suggested a phylogenetic closeness
463 between the Korean lineage and *M. fuscata*, is not necessarily conclusive. In particular, *M.*
464 *thibetana* should remain a candidate for being the sister taxon of the Korean lineage, because
465 *M. thibetana* is somewhat similar to the Korean fossil in terms of zygomaxillary shape,
466 particularly when size is adjusted. Further studies with a larger sample size, which ideally
467 include only wild-caught specimens, will clarify our findings.

468 **5. Conclusion**

469 This study investigated the zygomaxillary morphology of the fossil macaque from the
470 Middle to Late Pleistocene of the Korean Peninsula compared with living macaque species.
471 We found that the Korean fossil is the most similar in zygomaxillary morphology to *M.*
472 *fuscata*, followed by *M. mulatta*, and is phylogenetically related to the clade that includes *M.*

mulatta, *M. cyclopis*, and *M. fuscata* (particularly to *M. fuscata*). This finding, unlike traditional scenarios, suggests that the morphological characteristics of *M. fuscata* could have been formed before this group dispersed to the Japanese archipelago, potentially shedding light on how primates adapted to a cold environment.

Acknowledgments

We would like to convey our gratitude to JY Seong, SY Lee, BI Yun, KW Lee, and the staff of the Chungbuk Natural History Museum and the Institute of Korean Prehistory for their help with accessing the fossil specimens and for providing information about them, and C. Dongwoo and Y. Lee for their assistance with CT scanning of the specimens. We also thank Tet. Hayashi, Ter. Hayashi, S. Yachimori, E. Ashida, D. Shimizu, T. Takano, Y. Shintaku, H. Taru, H. Hirotani, H. Takahashi, N. Shigehara, and many field workers for collecting/preserving the remains of macaques and/or permitting us to access the collections that they manage. We thank N. Ogihara, S. Kondo, M. Nakatsukasa, Thaung Htike, Zin-Maung-Maung-Thein, and W. Yano for their help with CT scanning of extant species and N. Egi for her help with the 3D surface modeling. We thank three anonymous reviewers and editors for their constructive comments on our previous version of this manuscript, which

considerably improved the clarity of this paper. We thank the Smithsonian's Division of Mammals (Dr. Kristofer Helgen) and Human Origins Program (Dr. Matt Tocheri) for the scans of USNM specimens used in this research (http://humanorigins.si.edu/evidence/3d-collection/primate). These scans were acquired through the generous support of the Smithsonian 2.0 Fund and the Smithsonian's Collections Care and Preservation Fund. Lynn Copes, Lynn Lucas, and the MCZ provided access to these scans, originally appearing in Copes and Kimbel (2016) and Copes et al. (2016), funding for the collection of which was provided by NSF DDIG #0925793, and a Wenner-Gren Foundation Dissertation Grant #8102 (both to Lynn Copes). These scans were downloaded from MorphoSource.org, a web-accessible archive for 3D digital data housed by Duke University. This study was funded by the Fujiwara Natural History Foundation (to TI), the Keihanshin Consortium for Fostering the Next Generation of Global Leaders in Research (K-CONNEX) (to TI), and JSPS grants-in-aid for Scientific Research (Grant 26650171 to TDN).

References

Albrecht, G.H., 1978. The Craniofacial Morphology of the Sulawesi Macaques: Multivariate Approaches to Biological Problems. Contributions to Primatology 13,. Karger, Basel.

505 Arnold, C., Matthews, L.J., Nunn, C.L., 2010. The 10 k Trees Website: A new online resource
506 for primate phylogeny. Evolutionary Anthropology 19, 114-118.
507 Bouckaert, R., Heled, J., Kuhnert, D., Vaughan, T., Wu, C.H., Xie, D., Suchard, M.A., Rambaut,
508 A., Drummond, A.J., 2014. BEAST 2: a software platform for Bayesian evolutionary
509 analysis. PLoS Computational Biology 10, e1003537.
510 Bouckaert, R., 2015. bModelTest: Bayesian site model selection for nucleotide data. bioRxiv,
511 020792.
512 Cardini, A., Elton, S., 2007. Sample size and sampling error in geometric morphometric studies
513 of size and shape. Zoomorphology 126, 121-134.
514 Catalano, S.A., Goloboff, P.A., Giannini, N.P., 2010. Phylogenetic morphometrics (I): the use
515 of landmark data in a phylogenetic framework. Cladistics 26, 539-549.
516 Catalano, S.A., Torres, A., 2016. Phylogenetic inference based on landmark data in 41
517 empirical data sets. Zoological Scripta 46, 1-11.
518 Chakraborty, D., Ramakrishnan, U., Panor, J., Mishra, C., Sinha, A., 2007. Phylogenetic
519 relationships and morphometric affinities of the Arunachal macaque *Macaca munzala*, a
520 newly described primate from Arunachal Pradesh, northeastern India. Molecular
521 Phylogenetics and Evolution 44, 838-849.

522 Chu, J.H., Lin, Y.S., Wu, H.Y., 2007. Evolution and dispersal of three closely related macaque
523 species, *Macaca mulatta*, *M. cyclopis*, and *M. fuscata*, in the eastern Asia. Molecular
524 Phylogenetics and Evolution 43, 418-429.
525 Copes, L.E., Kimbel, W.H., 2016. Cranial vault thickness in primates: *Homo erectus* does not
526 have uniquely thick vault bones. Journal of Human Evolution 90, 120-134.
527 Copes, L.E., Lucas, L.M., Thostenson, J.O., Hoekstra, H.E., Boyer, D.M., 2016. A collection
528 of non-human primate computed tomography scans housed in MorphoSource, a repository
529 for 3D data. Scientific Data 3, 160001.
530 Delson, E., 1977. Vertebrate paleontology, especially of nonhuman primates, in China. In:
531 Howells, W.W., Tsuchitani, P.J. (Eds.), Paleoanthropology in the People's Republic of
532 China. National Academy of Science, Washington, D.C., pp. 40-65.
533 Delson, E., 1980. Fossil macaques, phyletic relationships and a scenario of deployment. In:
534 Lindburg, D.G. (Ed.), The Macaques: Studies in Ecology, Behavior and Evolution.
535 Nostrand-Reinhold, New York, pp. 10-30.
536 Drake, A.G., Klingenberg, C.P., 2008. The pace of morphological change: historical
537 transformation of skull shape in St Bernard dogs. Proceedings of the Royal Society of
538 London B: Biological Sciences 275, 71-76.

539 Dryden, I.L., 2016. shapes: Statistical Shape Analysis. R package version 1.1-13. https://cran.r-
540 project.org/package=shapes.
541 Fan, P., Liu, Y., Zhang, Z., Zhao, C., Li, C., Liu, W., Liu, Z., Li, M., 2016. Phylogenetic position
542 of the white-cheeked macaque (*Macaca leucogenys*), a newly described primate from
543 Southeastern Tibet. Molecular Phylogenetics and Evolution 107, 80-89.
544 Fleagle, J.G., 2013. Primate Adaptation and Evolution. 3rd edn. Academic Press, San Diego.
545 Fooden, J., 1982. Taxonomy and evolution of the *sinica* group of macaques: 3. Species and
546 subspecies accounts of *Macaca assamensis*. Fieldiana Zoology 10, 1-52.
547 Fooden, J., 1983. Taxonomy and evolution of the *sinica* group of macaques: 4. Species account
548 of *Macaca thibetana*. Fieldiana Zoology 17, 1-20.
549 Fooden, J., 1988. Taxonomy and evolution of the *sinica* group of macaques: 6. Interspecific
550 comparisons and synthesis. Fieldiana Zoology 45, 1-44.
551 Fooden, J., 1990. The bear macaques, *Macaca arctoides*: a systematic review. Journal of
552 Human Evolution 19, 607-686.
553 Fooden, J., 2000. Systematic review of the rhesus macaques, *Macaca mulatta* (Zimmermann,
554 1780). Fieldiana Zoology 96, 1-180.
555 Fooden, J., Aimi, M., 2005. Systematic review of Japanese macaques, *Macaca fuscata* (Gray,

556 1870). Fieldiana Zoology 104, 1-198.

557 Fooden, J., 2006. Comparative review of *fascicularis*-group species of macaques (Primates:

558 *Macaca*). Fieldiana Zoology 107, 1-44.

559 Frost, S.R., Marcus, L.F., Bookstein, F.L., Reddy, D.P., Delson, E., 2003. Cranial allometry,

560 phylogeography, and systematics of large-bodied papionins (primates: Cercopithecinae)

561 inferred from geometric morphometric analysis of landmark data. Anatatomical Record

562 275A, 1048-1072.

563 Gilbert, C.C., 2011. Phylogenetic analysis of the African papionin basicranium using 3-D

564 geometric morphometrics: the need for improved methods to account for allometric effects.

565 American Journal of Physical Anthropology 144, 60-71.

566 Gilbert, C.C., Grine, F.E., 2010. Morphometric variation in the papionin muzzle and the

567 biochronology of the South African Plio-Pleistocene karst cave deposits. American

568 Journal of Physical Anthropology 141, 418-429.

569 Gilbert, C.C., Rossie, J.B., 2007. Congruence of molecules and morphology using a narrow

570 allometric approach. Proceedings of the National Academy of Sciences of the United

571 States of America 104, 11910-11914.

572 Gilbert, C.C., Frost, S.R., Strait, D.S., 2009. Allometry, sexual dimorphism, and phylogeny: a

573 cladistic analysis of extant African papionins using craniodental data. Journal of Human
574 Evolution 57, 298-320.
575 Goloboff, P., 2003. Improvements to resampling measures of group support. Cladistics 19, 324-
576 332.
577 Goloboff, P.A., Catalano, S.A., 2011. Phylogenetic morphometrics (II): algorithms for
578 landmark optimization. Cladistics 27, 42-51.
579 Goloboff, P.A., Catalano, S.A., 2016. TNT version 1.5, including a full implementation of
580 phylogenetic morphometrics. Cladistics 32, 221-238.
581 Goloboff, P.A., Farris, J.S., Nixon, K.C., 2008. TNT, a free program for phylogenetic analysis.
582 Cladistics 24, 774-786.
583 Gunz, P., Mitteroecker, P., Bookstein, F.L., 2005. Semilandmarks in three dimensions. In: Slice,
584 D.E. (Ed.), Modern Morphometrics in Physical Anthropology. Kluwer Academic
585 Publishers, New York, pp. 73-98.
586 Hanya, G., Menard, N., Qarro, M., Ibn Tattou, M., Fuse, M., Vallet, D., Yamada, A., Go, M.,
587 Takafumi, H., Tsujino, R., Agetsuma, N., Wada, K., 2011. Dietary adaptations of
588 temperate primates: comparisons of Japanese and Barbary macaques. Primates 52, 187-
589 198.

590 Ito, T., Nishimura, T.D., 2016. Enigmatic diversity of the maxillary sinus in macaques and its
591 possible role as a spatial compromise in craniofacial modifications. Evolutionary Biology
592 43, 414-426.
593 Ito, T., Nishimura, T.D., Senut, B., Koppe, T., Treil, J., Takai, M., 2009. Reappraisal of *Macaca*
594 *speciosa subfossilis* from the late Pleistocene of northern Vietnam based on the analysis
595 of cranial anatomy. International Journal of Primatology 30, 646-661.
596 Ito, T., Nishimura, T., Takai, M., 2014a. Ecogeographical and phylogenetic effects on
597 craniofacial variation in macaques. American Journal of Physical Anthropology 154, 27-
598 41.
599 Ito, T., Nishimura, T.D., Ebbestad, J.O.R., Takai, M., 2014b. Computed tomography
600 examination of the face of *Macaca anderssoni* (Early Pleistocene, Henan, northern China):
601 implications for the biogeographic history of Asian macaques. Journal of Human
602 Evolution 72, 64-80.
603 Ito, T., Nishimura, T.D., Hamada, Y., Takai, M., 2015. Contribution of the maxillary sinus to
604 the modularity and variability of nasal cavity shape in Japanese macaques. Primates 56,
605 11-19.
606 Jablonski, N.G., Pan, Y., 1988. The evolution and palaeobiogeography of monkeys in China.

In: Whyte, P., Aigner, J., Jablonski, N.G., Taylor, G., Walker, D., Wang, P.X. (Eds.), The Palaeoenvironment of East Asia from the Mid-Tertiary. Centre of Asian Studies, Hong Kong, pp. 849-867.

Jiang, J., Yu, J., Li, J., Li, P., Fan, Z., Niu, L., Deng, J., Yue, B., 2016. Mitochondrial genome and nuclear markers provide new insight into the evolutionary history of macaques. PLoS ONE 11, e0154665.

Karen J, W., 2011. Climatic and altitudinal influences on variation in *Macaca* limb morphology. Anatomy Research International 2011, 1-18.

Katoh, K., Standley, D.M., 2013. MAFFT multiple sequence alignment software version 7: improvements in performance and usability. Molecular Biolology and Evolution 30, 772-780.

Klingenberg, C.R., 2011. MorphoJ: an integrated software package for geometric morphometrics. Molecular Ecology Resources 11, 353-357.

Lee, Y.-J. (Ed.), 2006. The Paleolithic Culture of Jungwon Region, Korea. Institute for Jungwon Culture, Chungbuk National University, Cheongju [Korean with English abstracts].

Lee, Y.-J., Takai, M., 2012. The Middle to Late Pleistocene macaque fossils from central Korea.

In: Drozdov, N.I., Lee, Y.-J., Woo, J.-Y. (Eds.), The 17th International Symposium: Suyanggae and Her Neighbors in Kurtak. Institute of Korean Prehistory and Krasnoyarsk State Pedagogical University, Cheongju, pp. 116–119.

Lee, Y.-J., Woo, J.-Y. (Eds.), 2005. Paleolithic Sites of the Jungwon Region, Korea. Chungbuk National History Museum, Chungbuk [Korean with English abstracts].

Lee, Y.-J., Woo, J.-Y., Lee, S.-W., Byeong-Il, Y., Park, J.-Y., 2013. Progress Report of Gunang Cave Site, Danyang (IV) – 2011 Year Excavation (5th). Institute of Korean Prehistory Danyang County-Research Report 38 [Korean with English abstract].

Li, C., Zhao, C., Fan, P.F., 2015. White‐cheeked macaque (*Macaca leucogenys*): A new macaque species from Modog, southeastern Tibet. American Journal of Primatology 77, 753-766.

Li, J., Han, K., Xing, J., Kim, H.S., Rogers, J., Ryder, O.A., Disotell, T., Yue, B., Batzer, M.A., 2009. Phylogeny of the macaques (Cercopithecidae: *Macaca*) based on Alu elements. Gene 448, 242-249.

Liedigk, R., Roos, C., Brameier, M., Zinner, D., 2014. Mitogenomics of the Old World monkey tribe Papionini. BMC Evolutionary Biology 14, 176.

Márquez, S., Laitman, J.T., 2008. Climatic effects on the nasal complex: a CT imaging,

comparative anatomical, and morphometric investigation of *Macaca mulatta* and *Macaca fascicularis*. Anatomical Record 291, 1420-1445.

Mitteroecker, P., Bookstein, F., 2011. Linear discrimination, ordination, and the visualization of selection gradients in modern morphometrics. Evolutionary Biology 38, 100-114.

Monteiro, L.R., 1999. Multivariate regression models and geometric morphometrics: the search for causal factors in the analysis of shape. Systematic Biology 48, 192-199.

Morales, J.C., Melnick, D.J., 1998. Phylogenetic relationships of the macaques (Cercopithecidae: *Macaca*), as revealed by high resolution restriction site mapping of mitochondrial ribosomal genes. Journal of Human Evolution 34, 1-23.

Nishimura, T.D., Ito, T., Yano, W., Ebbestad, J.O.R., Takai, M., 2014. Nasal architecture in *Procynocephalus wimani* (Early Pleistocene, China) and implications for its phyletic relationship with *Paradolichopithecus*. Anthropological Science 122, 101-113.

Noback, M.L., Harvati, K., Spoor, F., 2011. Climate-related variation of the human nasal cavity. American Journal of Physical Anthropology 145, 599-614.

Pan, R., Yanzhang, P., 1995. Body size of *Macaca anderssoni* and its offspring. Human Evolution 10, 283-287.

Pan, Y.R., Jablonski, N.G., 1987. The age and geographical distribution of fossil cercopithecids

658 in China. Human Evolution 2, 59-69.
659 Park, S., Lee, Y., 1998. Pleistocene faunal remains from Saekul/Chonyokul at Turupong cave
660 complex with special emphasis on the large mammalian fossils. In: Xu, Q., Lee, Y. (Eds.),
661 International Symposium for the Celebration of Chinese Academician Jia Lanpo's 90th
662 Birthday: Suyanggae and Her Neighbours. Science Press, Beijing, pp. 55-70.
663 Pearson, A., Groves, C., Cardini, A., 2015. The 'temporal effect'in hominids: Reinvestigating
664 the nature of support for a chimp-human clade in bone morphology. Journal of Human
665 Evolution 88, 146-159.
666 Perelman, P., Johnson, W.E., Roos, C., Seuánez, H.N., Horvath, J.E., Moreira, M.A., Kessing,
667 B., Pontius, J., Roelke, M., Rumpler, Y., 2011. A molecular phylogeny of living primates.
668 PLoS Genetetics 7, e1001342.
669 R Core Team, 2017. R: A language and environment for statistical computing, R foundation
670 for Statistical Computing, Vienna.
671 Rae, T.C., Hill, R.A., Hamada, Y., Koppe, T., 2003. Clinal variation of sinus volume in
672 Japanese macaques (*Macaca fuscata*). American Journal of Primatology 59, 153-158.
673 Rae, T.C., Vidarsdottir, U.S., Jeffery, N., Steegmann, A.T., 2006. Developmental response to
674 cold stress in cranial morphology of *Rattus*: implications for the interpretation of climatic

675 adaptation in fossil hominins. Proceedings of the Royal Society of London B: Biological
676 Sciences 273, 2605-2610.
677 Schillaci, M.A., Schillaci, M.E., 2009. Estimating the probability that the sample mean is within
678 a desired fraction of the standard deviation of the true mean. Journal of Human Evolution
679 56, 134-138.
680 Schlager, S., 2017. Morpho and Rvcg – Shape Analysis in R. In: Zheng, G., Li, S., Szekely, G.
681 (Eds.), Statistical Shape and Deformation Analysis. Academic Press, New York, pp. 217-
682 256.
683 Schlosser, M., 1924. Fossil primates from China. Palaeontologia Sinica Series C 1, 1-16.
684 Sibal, L.R., Samson, K.J., 2001. Nonhuman primates: a critical role in current disease research.
685 ILAR Journal 42, 74-84.
686 Sidlauskas, B., 2008. Continuous and arrested morphological diversification in sister clades of
687 characiform fishes: a phylomorphospace approach. Evolution 62, 3135-3156.
688 Simons, E.L., 1970. The deployment and history of Old World monkeys (Cercopithecidae,
689 Primates). In: Napier, J.R., Napier, P.H. (Eds.), Old World Monkeys: Evolution,
690 Systematics, and Behavior. Academic Press, New York, pp. 97-137.
691 Singleton, M., 2002. Patterns of cranial shape variation in the Papionini (Primates:

692 Cercopithecinae). Journal of Human Evolution 42, 547-578.
693 Sinha, A., Datta, A., Madhusudan, M.D., Mishra, C., 2005. *Macaca munzala*: A new species
694 from Western Arunachal Pradesh, Northeastern India. International Journal of
695 Primatology 26, 977-989.
696 Takai, M., Maschenko, E.N., Nishimura, T.D., Anezaki, T., Suzuki, T., 2008. Phylogenetic
697 relationships and biogeographic history of *Paradolichopithecus suskini* Trofimov 1977, a
698 large-bodied cercopithecus monkey from the Pliocene of Eurasia. Quaternery International
699 179, 108-119.
700 Tosi, A.J., Morales, J.C., Melnick, D.J., 2000. Comparison of Y chromosome and mtDNA
701 phylogenies leads to unique inferences of macaque evolutionary history. Molecular
702 Phylogenetetics and Evolution 17, 133-144.
703 Tsuji, Y., Hanya, G., Grueter, C.C., 2013. Feeding strategies of primates in temperate and alpine
704 forests: comparison of Asian macaques and colobines. Primates 54, 201-215.
705 Young, C.C., 1934. On the Insectivora, Chiroptera, Rodentia and Primates other than
706 *Sinanthropus* from locality 1 at Choukoutien. Palaeontologia Sinica Series C 8, 1-139.
707 Zhang, Z., Wei, H., Xu, Z., 1986. Mammalian fossils. In: City, M.o.L.P.a.M.o.B. (Ed.),
708 Miaohoushan: A Site of Early Paleolithic in Benxi Country, Liaoning. Wenwu Press,

709 Beijing, pp. 35–66 (in Chinese).

710

711

712 **Figure legends**

713 **Figure 1.** The zygomaxillary specimen (2ㅜㄷ-12-2169) from the Durubong Cave Complex
714 (Site 2), South Korea. (a) Left lateral view, (b) right lateral view, (c) occlusal view, and
715 (d) dorsal view. The scale is in centimeters.

716 **Figure 2.** (a) Original surface model and (b) corrected surface model of the Durubong specimen.
717 The arrows denote fixing of the orientation of fragments (green and blue regions) and
718 filling of gaps in the main body (red region).

719 **Figure 3.** Landmarks used in this study. (a) Frontal view, (b) dorsal view, (c) left lateral view,
720 and (d) occlusal view. Anatomically defined landmarks: red; curve semi-landmarks:
721 blue; and surface semi-landmarks: green (see also SOM Table S4).

722 **Figure 4.** Coronal computed tomography (CT) images at the level of M^1 in extant macaques.
723 (a–d) Species of the *sinica* group. Arrows denote the degree of lateral

expansion/constriction of the nasal cavity and the thickness of the lateral bony wall of the maxilla. The scale is in centimeters. An asterisk denotes the maxillary sinus.

Figure 5. Coronal computed tomography (CT) image (bottom left) and corresponding line-drawn diagram at the level of M^1 (bottom right) in the Durubong fossil macaque specimen (2ㅜㄷ-12-2169). Upper image illustrates where the cross-section is located. The areas filled in gray and the dots on the line diagram indicate the bony structure and plaster, respectively. Arrows denote the limited expansion of the nasal cavity and the thick lateral bony wall of the maxilla. The scale is in centimeters.

Figure 6. Relationships between bgPC scores and the lnCS of the zygomaxillary region in the fossil macaque specimen and extant macaque species. (a) bgPC1 based on the raw shape data vs. lnCS, (b) bgPC2 based on the raw shape data vs. lnCS, (c) bgPC2 vs. bgPC1 based on the raw shape data, and (d) bgPC2 vs. bgPC1 based on the size-adjusted shape data. Red (dashed-dotted lines), *sinica* group; green (dashed lines), *fascicularis* group; blue (dotted lines), *silenus* group; yellow (solid lines), *sylvanus* group; black, the fossil specimen (2ㅜㄷ-12-2169).

Figure 7. Zygomaxillary shape changes along the bgPC axes. (a) Image of the fossil specimen

showing the locations of the polygons illustrated in this figure. (b) bgPC1 and (c) bgPC2 based on the raw shape data. (d) bgPC1 and (e) bgPC2 based on the size-adjusted shape data. The upper row represents the lateral views of the zygomaxillary region, while the lower column represents the dorsal views. The negative (left, blue) and positive (right, red) extremes, and their superimposition (middle) are shown.

Figure 8. Procrustes distances from the fossil macaque specimen (*Macaca* cf. *robusta*) to all examined individuals of extant species of macaques based on (a) the raw shape data and (b) the size-adjusted shape data. Color indicates the species group (see the legend of Fig. 6).

Figure 9. Phylomorphospace of (a) the raw shape data and (b) the size-adjusted shape data. Color indicates the species group (see the legend of Fig. 6). Gray-filled circles indicate the most recent common ancestor of all macaques.

Figure 10. Parsimonious phylogenetic trees inferred from the three-dimensional landmark data from the zygomaxillary region of the fossil macaque specimen (2┬ ⊏-12-2169) and extant species of macaques based on (a) the raw shape data with a monophyly constraint, (b) the size-adjusted shape data with a monophyly constraint, (c) the raw shape data

without a monophyly constraint, and (d) the size-adjusted shape data without a monophyly constraint. Numbers near the nodes indicate GC support value when the landmarks were resampled. Asterisk indicates the fossil specimen.

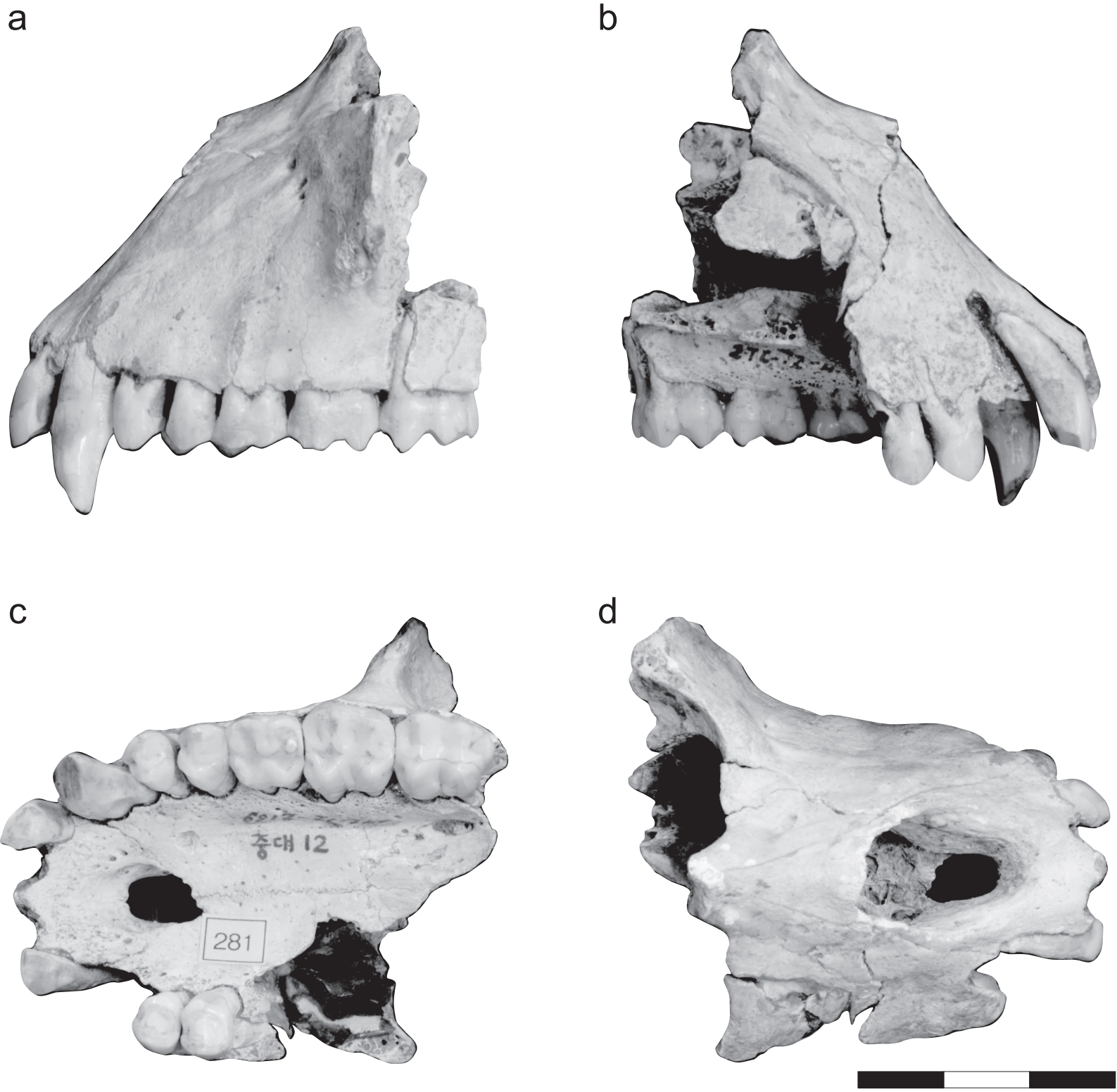
a
b
c
d
층대 12
281

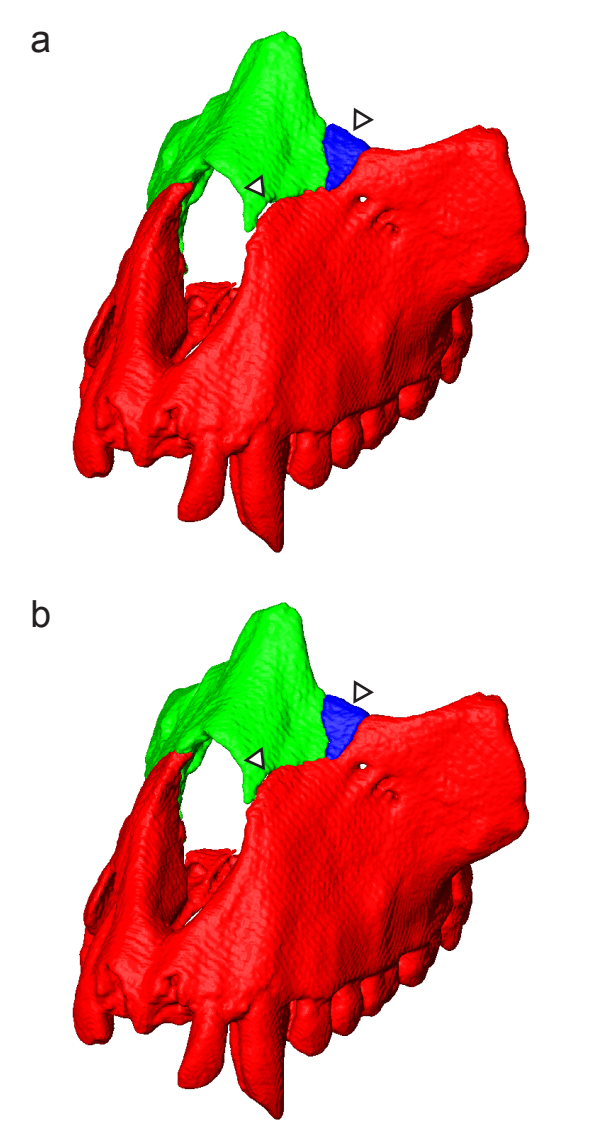
a
b

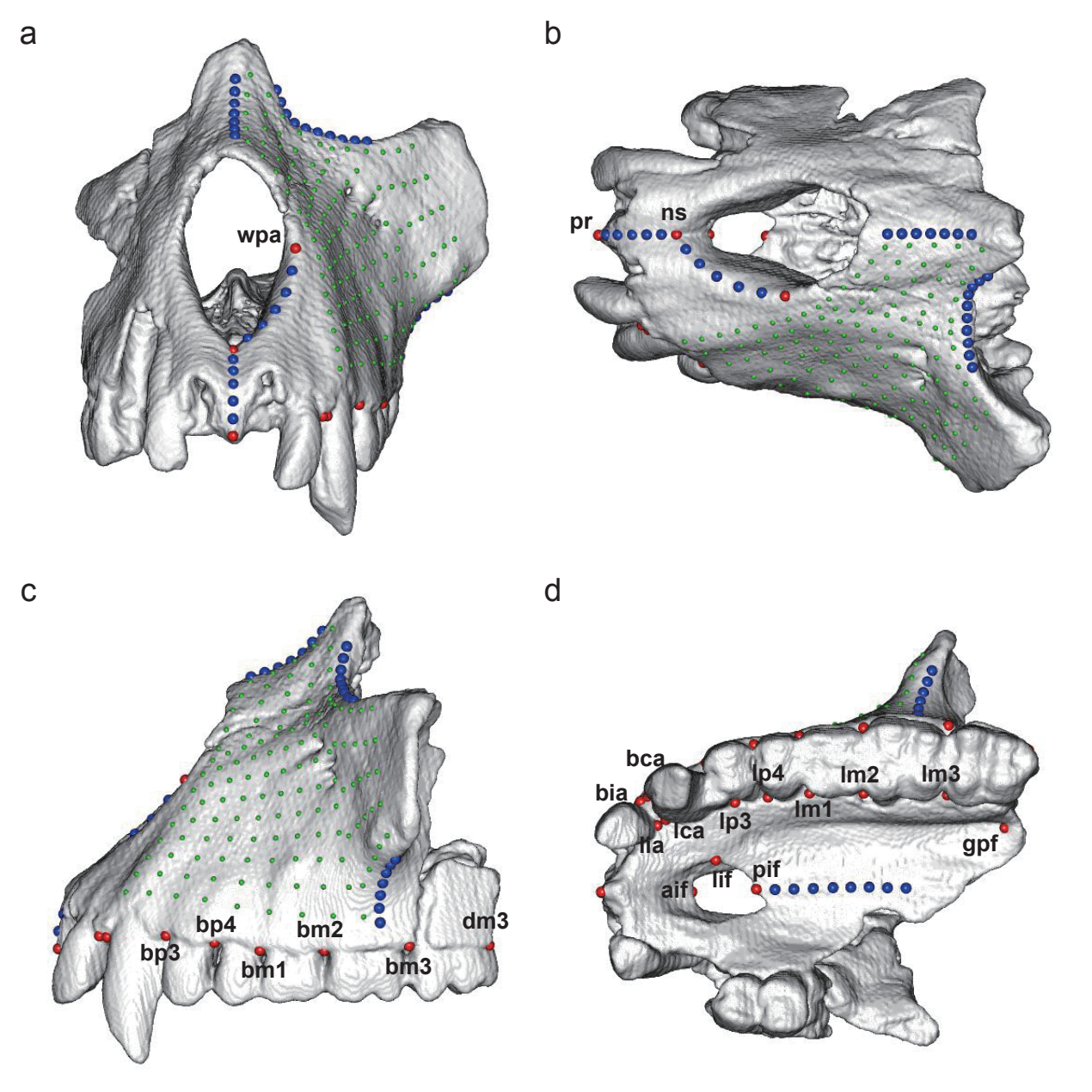
a
wpa
b
pr
ns
c
bp4
bm2
dm3
bp3
bm1
bm3
d
bca
lp4
lm2
lm3
bia
lm1
lp3
lca
lia
gpf
pif
aif
lif

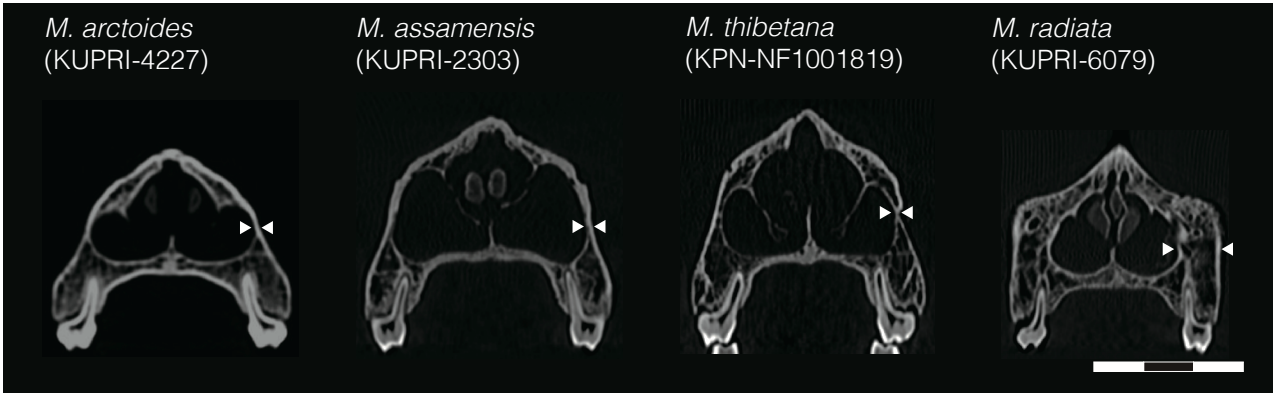
M. arctoides
(KUPRI-4227)
M. assamensis
(KUPRI-2303)
M. thibetana
(KPN-NF1001819)
M. radiata
(KUPRI-6079)
M. fuscata
(KUPRI-8886)
M. mulatta
(KUPRI-4408)
M. cyclopis
(DKY-1688)
M. fascicularis
(KUPRI-4703)

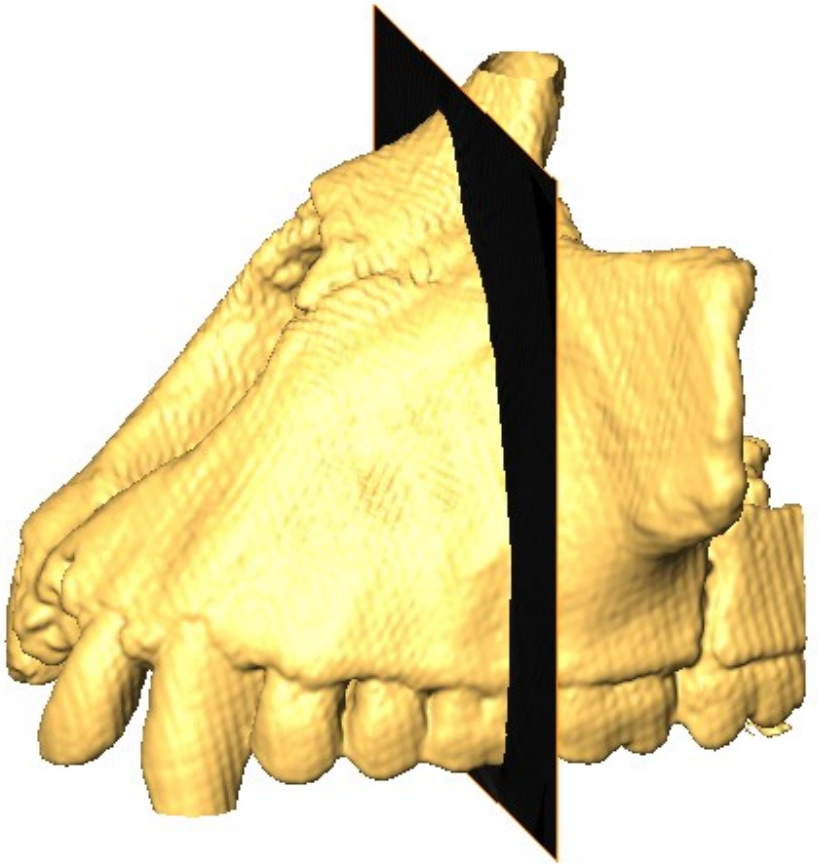

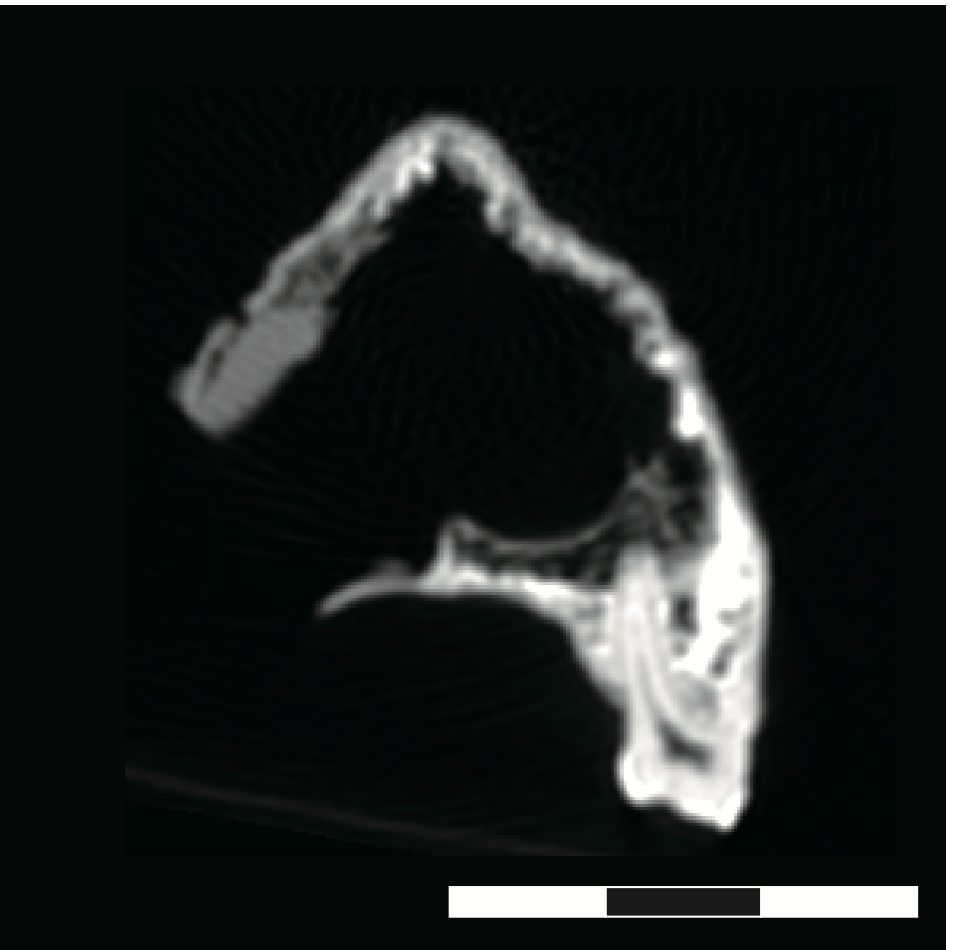

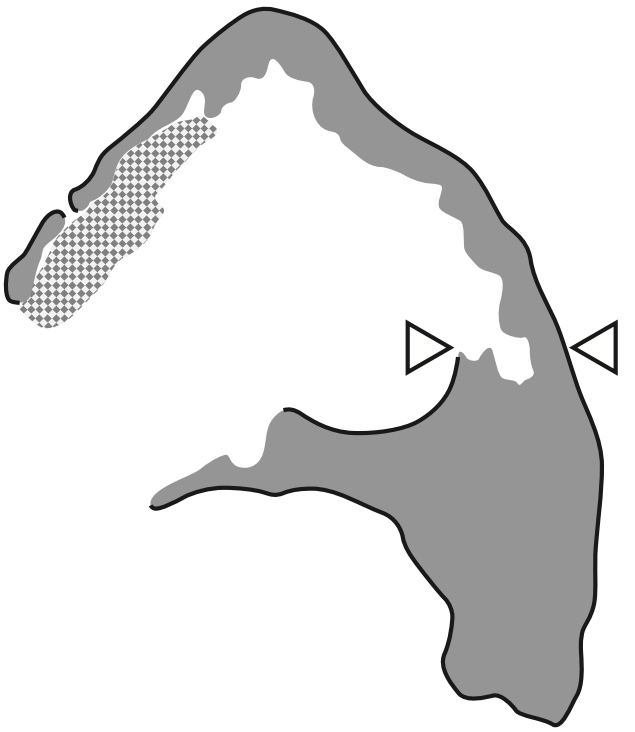

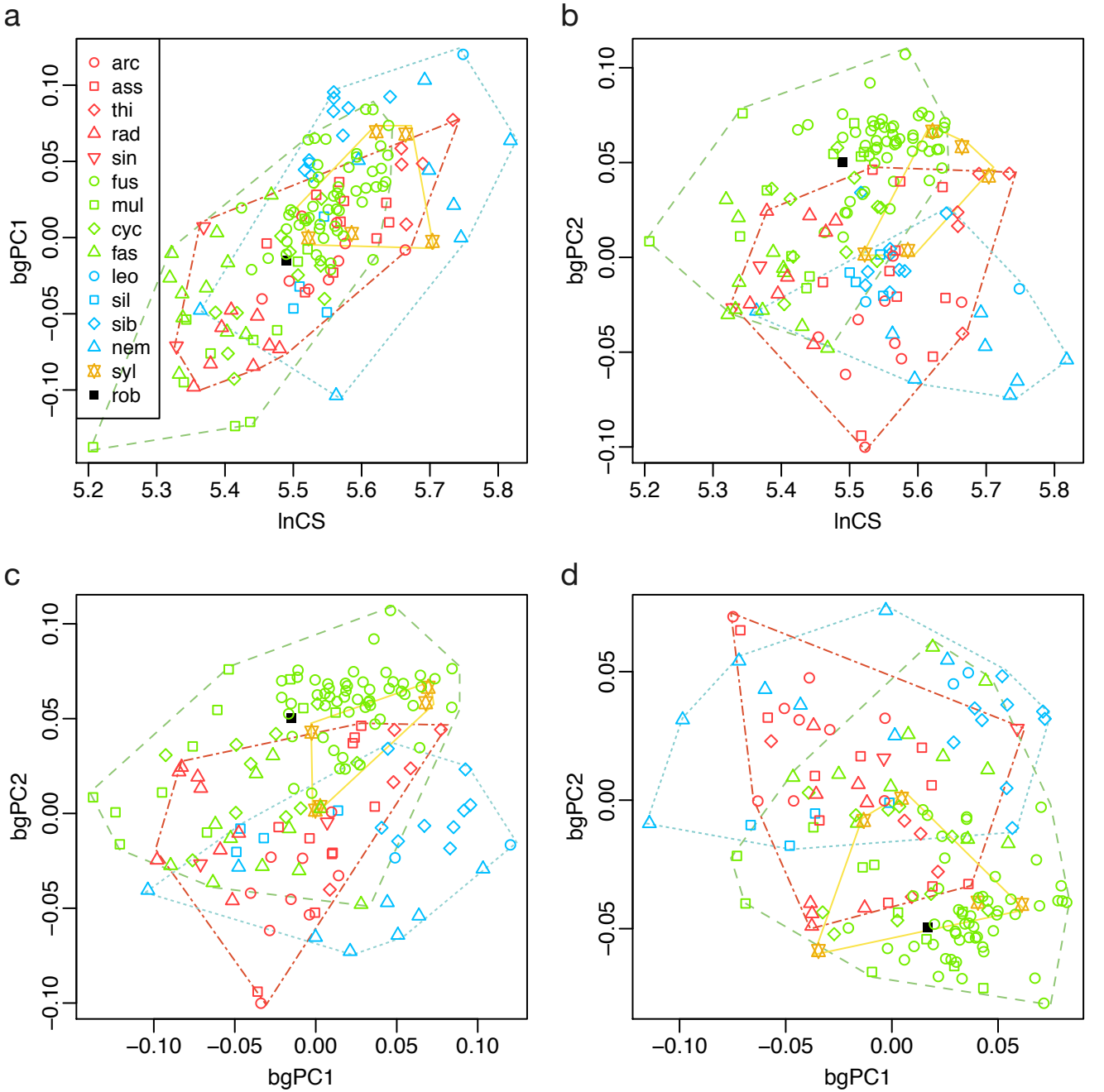
a
b
c
d
arc
ass
thi
rad
sin
fus
mul
cyc
fas
leo
sil
sib
nem
syl
rob
bgPC1
bgPC2
lnCS
5.2
5.3
5.4
5.5
5.6
5.7
5.8
0.10
0.05
0.00
−0.05
−0.10

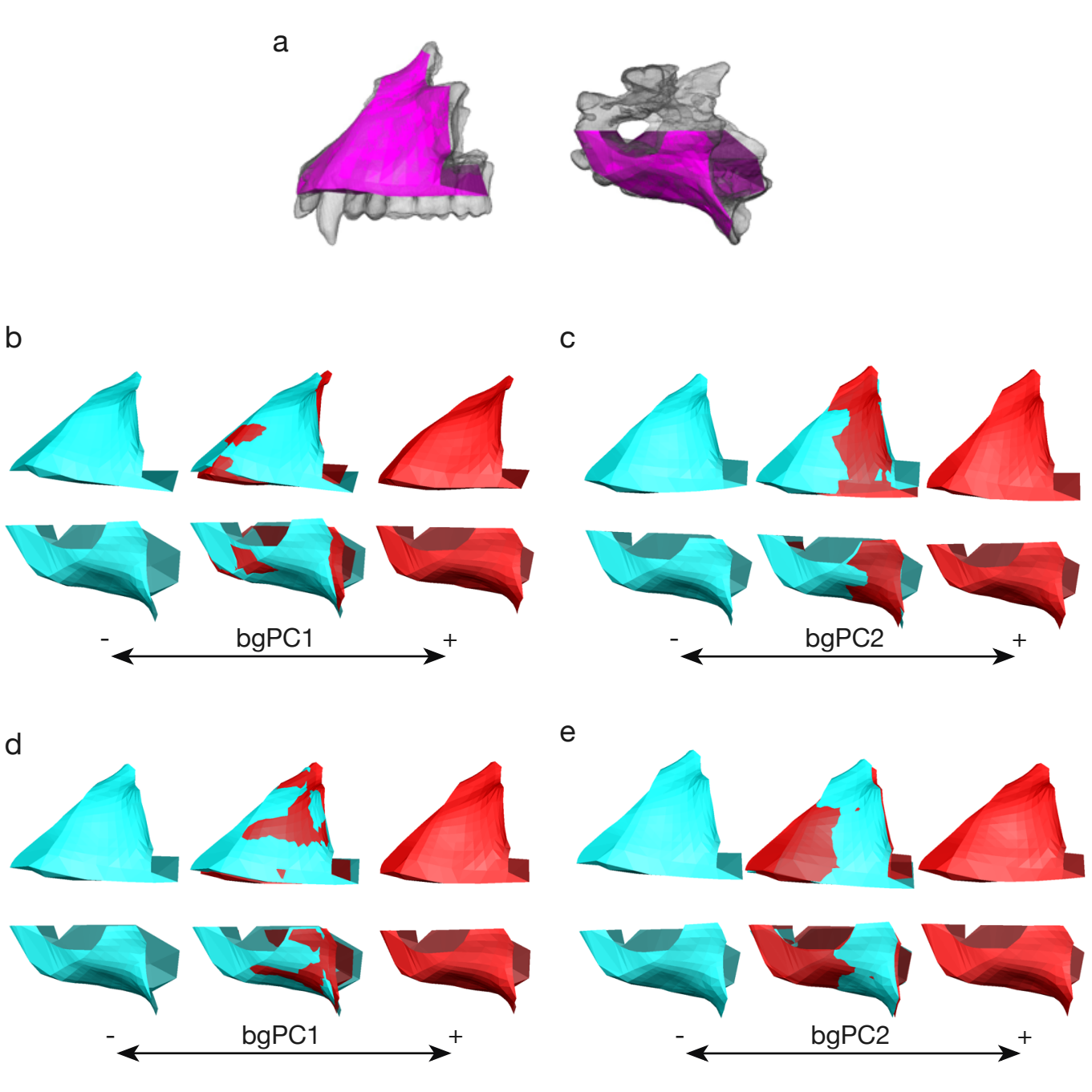
a
b
bgPC1
-
+
c
bgPC2
-
+
d
bgPC1
-
+
e
bgPC2
-
+

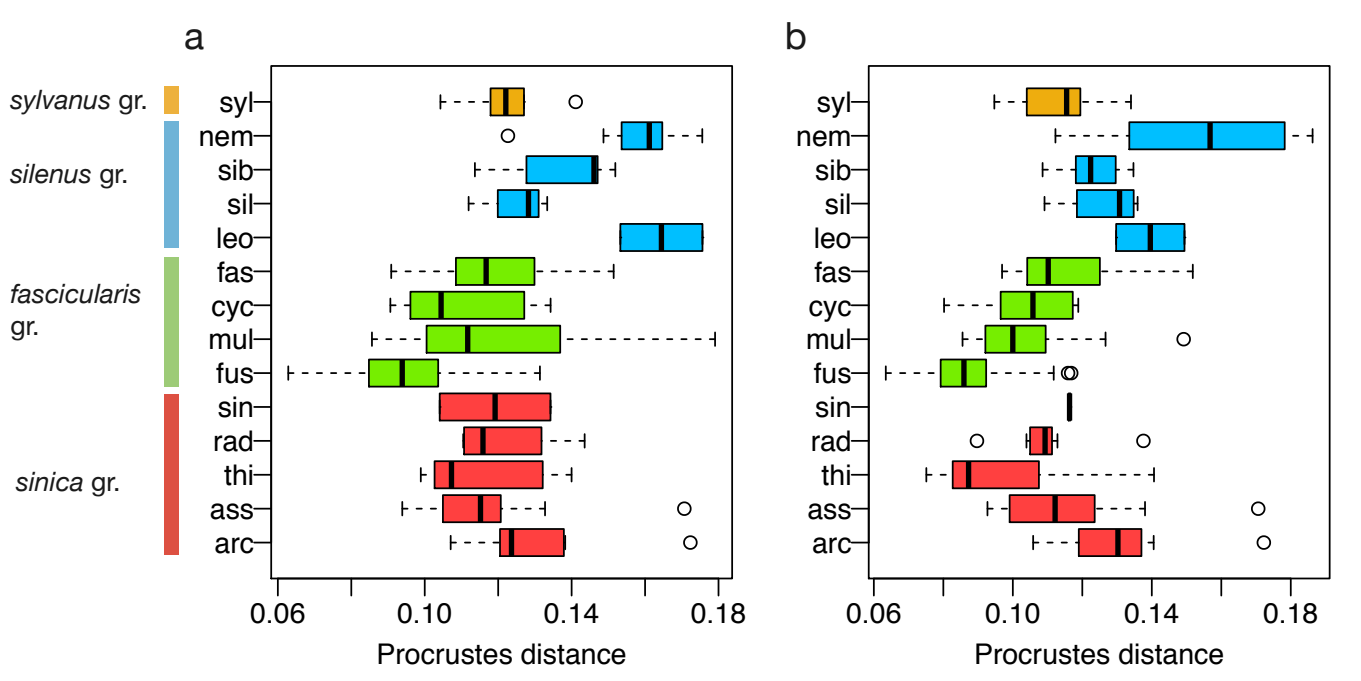
a
b
sylvanus gr.
silenus gr.
fascicularis gr.
sinica gr.
syl
nem
sib
sil
leo
fas
cyc
mul
fus
sin
rad
thi
ass
arc
0.06
0.10
0.14
0.18
Procrustes distance

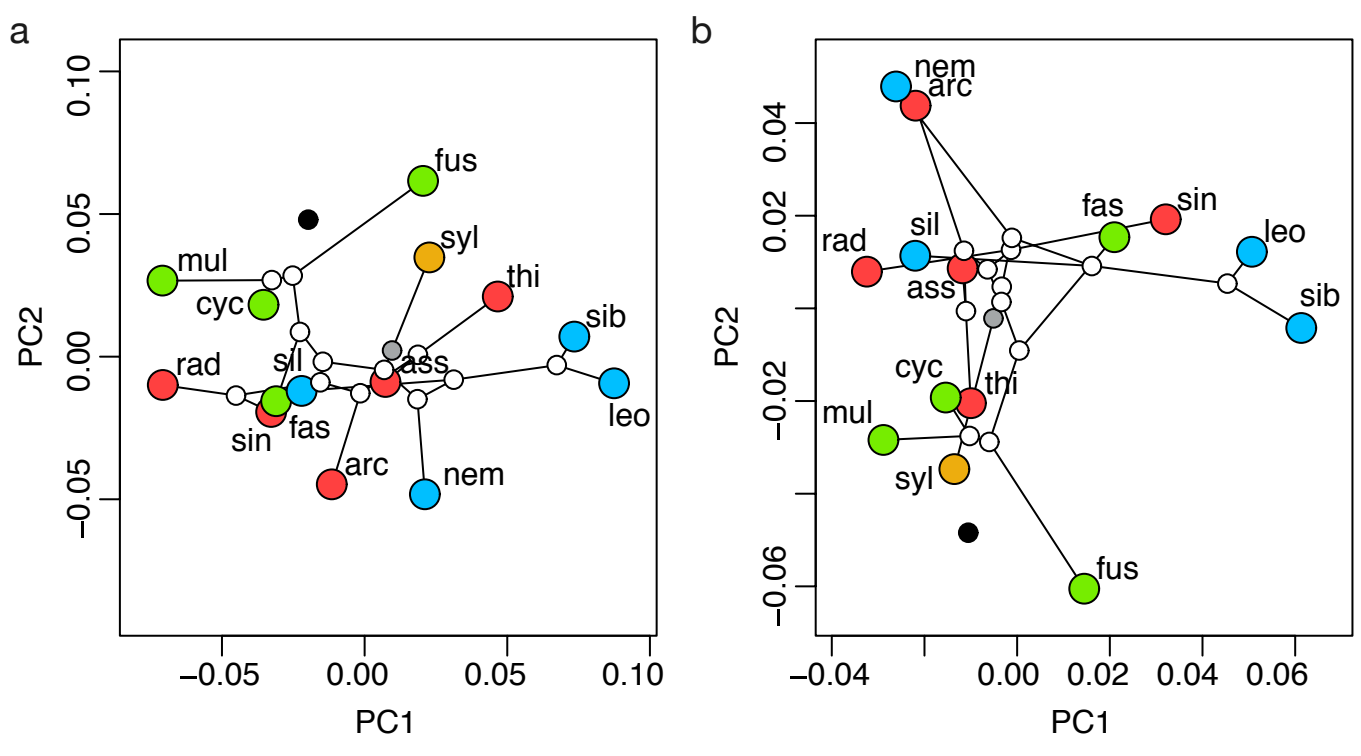
a
b
PC1
PC2
fus
syl
mul
thi
cyc
sib
rad
sil
ass
leo
sin
fas
arc
nem
0.10
0.05
0.00
−0.05
0.04
0.02
−0.02
−0.06
0.06

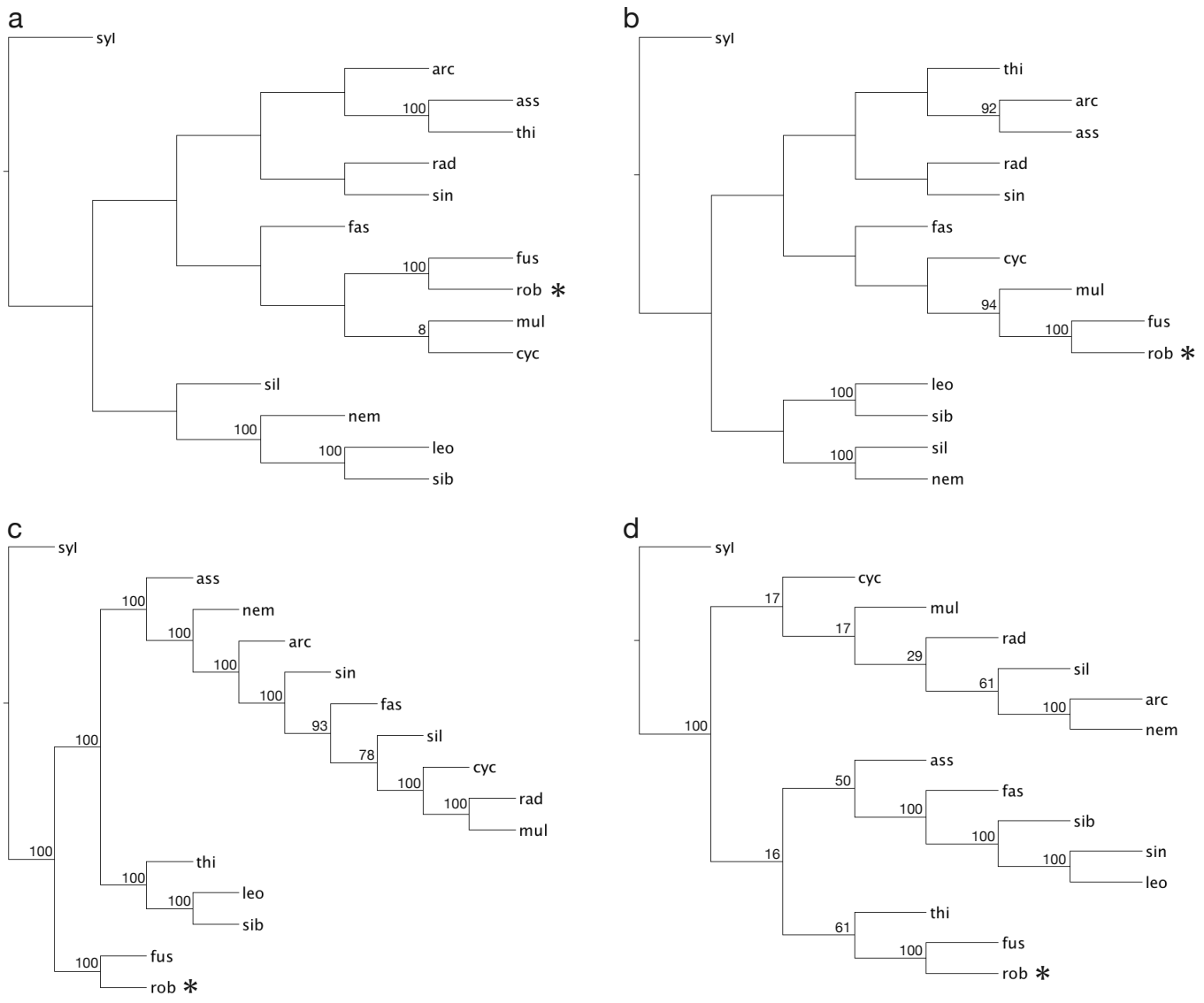
a
syl
arc
ass
100
thi
rad
sin
fas
fus
100
rob *
mul
8
cyc
sil
nem
100
leo
100
sib
b
syl
thi
92
arc
ass
rad
sin
fas
cyc
mul
94
fus
100
rob *
leo
100
sib
sil
100
nem
c
syl
ass
100
nem
100
arc
100
sin
100
fas
93
sil
78
cyc
100
rad
100
mul
100
thi
100
leo
100
sib
fus
100
rob *
d
syl
cyc
17
mul
17
rad
29
sil
61
arc
100
nem
100
ass
50
fas
100
sib
100
sin
16
leo
thi
61
fus
100
rob *

Table 1 The sample used in this study.

Species group	Species	Abbreviation	*n*
sinica group	*M. arctoides*	arc	9
	M. assamensis	ass	10
	M. thibetana	thi	5
	M. radiata	rad	8
	M. sinica	sin	2
fascicularis group	*M. fuscata*	fus	53
	M. mulatta	mul	11
	M. cyclopis	cyc	10
	M. fascicularis	fas	11
silenus group	*M. leonina*	leo	2
	M. silenus	sil	4
	M. siberu	sib	9
	M. nemestrina	nem	8
sylvanus group	*M. sylvanus*	syl	5

unknown	*M.* cf. *robusta*	rob	1

Table S2 Specimens used in this study.

Species	Institute[a]	Catalog number	ID for analysis	Data source[b]	Doi	Origin
M. arctoides	DKY	1473	DKY_1473	PRI CT		unknown
	JMC	3111	JMC_3111	PRI CT		captive
	NMNH	256825	NMNH_256825	Smithsonian 3D collection		wild
	PRI	1871	PRI_1871	KAS CT		captive
	PRI	2793	PRI_2793	PRI CT		captive
	PRI	291	PRI_291	PRI CT		captive
	PRI	4227	PRI_4227	KAS CT		unknown
	PRI	5846	PRI_5846	PRI CT		captive
	PRI	6434	PRI_6434	PRI CT		unknown
M. assamensis	PRI	1893	PRI_1893	PRI CT		wild
	PRI	2178	PRI_2178	KAS CT		unknown
	PRI	2208	PRI_2208	PRI CT		unknown
	PRI	2302	PRI_2302	PRI CT		unknown
	PRI	2303	PRI_2303	PRI CT		unknown
	PRI	3057	PRI_3057	PRI CT		captive
	PRI	4498	PRI_4498	PRI CT		unknown
	PRI	5015	PRI_5015	PRI CT		unknown
	PRI	5230	PRI_5230	KAS CT		unknown
	PRI	5342	PRI_5342	PRI CT		unknown

M. cyclopis	DKY	1688	DKY_1688	PRI CT	unknown
	NMNH	296795	NMNH_296795	Smithsonian 3D collection	wild
	PRI	1358	PRI_1358	PRI CT	unknown
	PRI	4201	PRI_4201	PRI CT	captive
	PRI	4233	PRI_4233	PRI CT	unknown
	PRI	4486	PRI_4486	PRI CT	wild
	PRI	528	PRI_528	PRI CT	captive
	PRI	5847	PRI_5847	PRI CT	unknown
	PRI	6431	PRI_6431	PRI CT	captive
	PRI	9520	PRI_9520	PRI CT	unknown
M. fascicularis	DKY	995	DKY_995	PRI CT	unknown
	NMNH	121511	NMNH_121511	Smithsonian 3D collection	wild
	NMNH	317191	NMNH_317191	Smithsonian 3D collection	wild
	NMNH	573504	NMNH_573504	Smithsonian 3D collection	wild
	PRI	3046	PRI_3046	PRI CT	unknown
	PRI	4434	PRI_4434	KAS CT	unknown
	PRI	4477	PRI_4477	PRI CT	unknown
	PRI	4478	PRI_4478	PRI CT	unknown
	PRI	4703	PRI_4703	PRI CT	unknown
	PRI	5225	PRI_5225	PRI CT	captive
	PRI	6680	PRI_6680	PRI CT	captive

M. fuscata	HMCZ	37709	HMCZ_37709	MorphoSource	doi:10.17602/M2/M3043	wild
	HNCC	03-10	HNCC_03-10	PRI CT		wild
	HNCC	04-14	HNCC_04-14	PRI CT		wild
	HNCC	04-60	HNCC_04-60	PRI CT		wild
	HNCC	05-16	HNCC_05-16	PRI CT		wild
	HNCC	05-17	HNCC_05-17	PRI CT		wild
	HNCC	05-43	HNCC_05-43	PRI CT		wild
	HNCC	06-23	HNCC_06-23	PRI CT		wild
	HNCC	06-40	HNCC_06-40	PRI CT		wild
	HNCC	06-59	HNCC_06-59	PRI CT		wild
	HNCC	06-60	HNCC_06-60	PRI CT		wild
	PRI	1571	PRI_1571	PRI CT		wild
	PRI	2168	PRI_2168	PRI CT		wild
	PRI	2586	PRI_2586	PRI CT		wild
	PRI	3452	PRI_3452	PRI CT		wild
	PRI	4076	PRI_4076	PRI CT		wild
	PRI	4113	PRI_4113	PRI CT		wild
	PRI	4335	PRI_4335	PRI CT		wild
	PRI	4338	PRI_4338	PRI CT		wild
	PRI	4341	PRI_4341	PRI CT		wild
	PRI	5868	PRI_5868	PRI CT		wild

PRI	6162	PRI_6162	PRI CT	wild
PRI	6470	PRI_6470	PRI CT	wild
PRI	6474	PRI_6474	PRI CT	wild
PRI	6498	PRI_6498	PRI CT	wild
PRI	6504	PRI_6504	PRI CT	wild
PRI	6833	PRI_6833	PRI CT	wild
PRI	7317	PRI_7317	PRI CT	wild
PRI	7381	PRI_7381	PRI CT	wild
PRI	7382	PRI_7382	PRI CT	wild
PRI	7385	PRI_7385	PRI CT	wild
PRI	8644	PRI_8644	PRI CT	wild
PRI	8658	PRI_8658	PRI CT	wild
PRI	8873	PRI_8873	PRI CT	wild
PRI	8885	PRI_8885	PRI CT	wild
PRI	8886	PRI_8886	PRI CT	wild
PRI	8889	PRI_8889	PRI CT	wild
PRI	8892	PRI_8892	PRI CT	wild
PRI	8893	PRI_8893	PRI CT	wild
PRI	8914	PRI_8914	PRI CT	wild
PRI	8974	PRI_8974	PRI CT	wild
PRI	9328	PRI_9328	PRI CT	wild

	PRI	9332	PRI_9332	PRI CT		wild
	PRI	9340	PRI_9340	PRI CT		wild
	PRI	9361	PRI_9361	PRI CT		wild
	SNC	H22-170	SNC_H22-170	PRI CT		wild
	SNC	H23-077	SNC_H23-077	PRI CT		wild
	SNC	H23-285	SNC_H23-285	PRI CT		wild
	TPM	M1656	TPM_M1656	PRI CT		wild
	TPM	M1889	TPM_M1889	PRI CT		wild
	TPM	M3958	TPM_M3958	PRI CT		wild
	TPM	M529	TPM_M529	PRI CT		wild
	TPM	M659	TPM_M659	PRI CT		wild
M. leonina	AMNH	MO-11090	AMNH_MO-11090	MorphoSource		wild
	NMNH	241022	NMNH_241022	Smithsonian 3D collection		wild
M. mulatta	DKY	1682	DKY_1682	PRI CT		unknown
	HMCZ	26475	HMCZ_26475	MorphoSource	doi:10.17602/M2/M3052	wild
	KAS	41	KAS_0041	KAS CT		captive
	PRI	218	PRI_218	PRI CT		captive
	PRI	2200	PRI_2200	PRI CT		unknown
	PRI	223	PRI_223	PRI CT		captive
	PRI	224	PRI_224	PRI CT		captive
	PRI	242	PRI_242	PRI CT		captive

	PRI	3523	PRI_3523	PRI CT	unknown
	PRI	4408	PRI_4408	PRI CT	captive
	PRI	580	PRI_580	PRI CT	captive
M. nemestrina	DKY	2110	DKY_2110	PRI CT	unknown
	NMNH	123144	NMNH_123144	Smithsonian 3D collection	wild
	NMNH	154367	NMNH_154367	Smithsonian 3D collection	wild
	PRI	1849	PRI_1849	PRI CT	unknown
	PRI	2299	PRI_2299	PRI CT	captive
	PRI	2454	PRI_2454	KAS CT	unknown
	PRI	3055	PRI_3055	KAS CT	unknown
	PRI	4225	PRI_4225	PRI CT	captive
M. radiata	JMC	1483	JMC_1483	KAS CT	captive
	PRI	3052	PRI_3052	PRI CT	unknown
	PRI	6079	PRI_6079	PRI CT	captive
	PRI	6684	PRI_6684	PRI CT	captive
	PRI	6685	PRI_6685	PRI CT	captive
	PRI	6686	PRI_6686	PRI CT	captive
	PRI	7140	PRI_7140	PRI CT	captive
	PRI	9532	PRI_9532	PRI CT	captive
M. siberu	NMNH	546835	NMNH_546835	Smithsonian 3D collection	wild
	PRI	1324	PRI_1324	PRI CT	wild

	PRI	1338	PRI_1338	PRI CT	wild
	PRI	1344	PRI_1344	PRI CT	wild
	PRI	1347	PRI_1347	PRI CT	wild
	PRI	5072	PRI_5072	PRI CT	wild
	PRI	5079	PRI_5079	PRI CT	wild
	PRI	5080	PRI_5080	PRI CT	wild
	PRI	5095	PRI_5095	PRI CT	wild
M. silenus	JMC	2488	JMC_2488	PRI CT	captive
	JMC	4864	JMC_4864	PRI CT	captive
	JMC	5740	JMC_5740	PRI CT	captive
	NMNH	574135	NMNH_574135	Smithsonian 3D collection	wild
M. sinica	NMNH	15259	NMNH_15259	Smithsonian 3D collection	wild
	PRI	1886	PRI_1886	PRI CT	wild
M. sylvanus	JMC	1392	JMC_1392	PRI CT	captive
	JMC	4798	JMC_4798	KAS CT	captive
	JMC	5644	JMC_5644	KAS CT	captive
	JMC	6330	JMC_6330	PRI CT	captive
	NMNH	255979	NMNH_255979	Smithsonian 3D collection	wild
M. thibetana	AMNH	M-84472	AMNH_M-84472	MorphoSource	wild
	JMC	5722	JMC_5722	PRI CT	captive
	KPM	NF1001819	KPM_NF1001819	PRI CT	unknown

	NMNH	241163	NMNH_241163	Smithsonian 3D collection	wild
	PRI	4230	PRI_4230	KAS CT	unknown
Unknown (*M.* cf. *robusta*)	CNUM	2ㅜㄷ-12-216	CNUM_2-12-2169	CNU CT	wild

[a] CNUM, the Chungbuk National University Museum, Chungcheongbuk-do, Korea; PRI, the Primate Research Institute, Kyoto University, Inuyama, Japan; JMC, the Japan Monkey Centre, Inuyama, Japan; KPM, the Kanagawa Prefectural Museum of Natural History, Odawara, Japan; DKY, the Department of Anatomy (Macro), Dokkyo Medical University, Mibu, Japan; KAS, the Laboratory of Physical Anthropology, Graduate School of Science, Kyoto University, Kyoto, Japan; AMNH, the American Museum of Natural History, New York, USA; NMNH, the National Museum of Natural History, Washington DC, USA; HMCZ, the Harvard Museum of Comparative Zoology, Cambridge, USA.

b PRI CT, the data scanned at the Primate Research Institute, Kyoto University, Inuyama, Japan; KAS CT, the data scanned at the the Laboratory of Physical Anthropology, Graduate School of Science, Kyoto University, Kyoto, Japan; CNU CT, the data scanned at the Chungbuk National University, Chungcheongbuk-do, Korea; the data downloaded from Smithsonian 3D collection (http://humanorigins.si.edu/evidence/3d-collection/primate); the data downloaded from MorphoSource (http://morphosource.org).

Table S3 Test for the differences in zygomaxillary shape among the different origins of specimens.

Response variable	Explanatory variable	R^2	SS	Df	F	*P*
All (wild, captive, and unknown-origin specimens)						
bgPC1 of raw shape data	Origin	0.009	0.001	2	0.59	0.556
	Species	0.488	0.138	14	8.92	< 0.001
	Residuals		0.145	131		
bgPC2 of raw shape data	Origin	0.007	0.001	2	0.47	0.628
	Species	0.626	0.136	14	15.69	< 0.001
	Residuals		0.081	131		
bgPC1 of size-adjusted shape data	Origin	0.044	0.005	2	3.02	0.052
	Species	0.303	0.045	14	4.07	< 0.001
	Residuals		0.103	131		
bgPC2 of size-adjusted shape data	Origin	0.039	0.002	2	2.63	0.076
	Species	0.670	0.124	14	18.96	< 0.001
	Residuals		0.061	131		
Procrustes coordinates of raw shape data	Origin	0.015	0.019	2	1.95	< 0.001
	Species	0.335	0.422	14	6.13	< 0.001
	Residuals		0.644	131		
Procrustes coordinates of size-adjusted shape data	Origin	0.021	0.021	2	2.44	< 0.001
	Species	0.304	0.314	14	5.15	< 0.001
	Residuals		0.571	131		

Subset (wild and captive specimens)						
bgPC1 of raw shape data	Origin	0.001	0.000	1	0.11	0.739
	Species	0.579	0.125	14	9.81	< 0.001
	Residuals		0.091	100		
bgPC2 of raw shape data	Origin	0.001	0.000	1	0.08	0.778
	Species	0.712	0.125	14	17.68	< 0.001
	Residuals		0.051	100		
bgPC1 of size-adjusted shape data	Origin	0.046	0.003	1	4.83	0.030
	Species	0.377	0.038	14	4.31	< 0.001
	Residuals		0.063	100		
bgPC2 of size-adjusted shape data	Origin	0.025	0.001	1	2.59	0.111
	Species	0.732	0.116	14	19.49	< 0.001
	Residuals		0.043	100		
Procrustes coordinates of raw shape data	Origin	0.013	0.012	1	2.763	< 0.001
	Species	0.398	0.382	14	6.184	< 0.001
	Residuals		0.441	100		
Procrustes coordinates of size-adjusted shape data	Origin	0.017	0.013	1	3.344	< 0.001
	Species	0.360	0.280	14	5.037	< 0.001
	Residuals		0.397	100		

ANOVA (Type II) was performed for the bgPC scores and Procrustes coordinates, wherein origin of specimen (captive, wild, and unknown) and species were used as explanatory variables. This was done for all sample and for the subset of sample (wild and captive). For these analyses, "procD.lm" function of "geomorph" package and "etasq" function of "heplots" package in R were used.

Table S4 Landmarks used in this study.

Abbreviation	Definition
Anatomically-defined landmarks	
wpa	Point corresponding to largest width of piriform aperture.
ns	Nasospinale.
aif	Antero-sperior point of incisive foramen.
pif	Posterior-most point of incisive foramen.
lif	Lateral-most point of incisive foramen.
pr	Prosthion.
bia	Postero-labial point of lateral incisor alveolus.
lia	Postero-lingual point of lateral incisor alveolus.
bca	Antero-labial point of canine alveolus.
lca	Antero-lingual point of canine alveolus.
bp3	Labial P^3: most mesial point on P^3 alveolus, projected labially onto alveolar margin.
lp3	Lingual P^3: most mesial point on P^3 alveolus, projected lingually onto alveolar margin.
bp4	Labial P^4: most mesial point on P^4 alveolus, projected labially onto alveolar margin.
lp4	Lingual P^4: most mesial point on P^4 alveolus, projected lingually onto alveolar margin.
bm1	Labial M^1: contact point between P^4 and M^1, projected labially onto alveolar margin.
lm1	Lingual M^1: contact point between P^4 and M^1, projected lingually onto alveolar margin.
bm2	Labial M^2: contact point between M^1 and M^2, projected labially onto alveolar margin.
lm2	Lingual M^2: contact point between M^1 and M^2, projected lingually onto alveolar margin.

bm3	Labial M^3: contact point between M^2 and M^3, projected labially onto alveolar margin.
lm3	Lingual M^3: contact point between M^2 and M^3, projected lingually onto alveolar margin.
dm3	Distal M^3: most posterior point on M^3 alveolus, projected labially onto alveolar margin.
gpf	Most posterior point on the margin of greater palatine foramen.
Semi-landmarks on curves	
	Eight points on the superior midline of nasal bone.
	Six points on the superior midline of premaxilla, which is between ns and pr.
	Seven points on the inferior midline of maxilla, which is from pif to approximately the meeting point of maxilla and palatine.
	Five points on the lateral margin of nasal aperture, which is between wpa and ns.
	Ten points on the inferior margin of orbital opening.
	Seven points on the inferior margin of zygomatic process.
Semi-landmarks on surface	
	One-hundred and thirty-two points on the lateral side of zygomaxilla.

Some of these definitions are in accordance with Cardini et al. (2007) and Ito and Nishimura (2016).

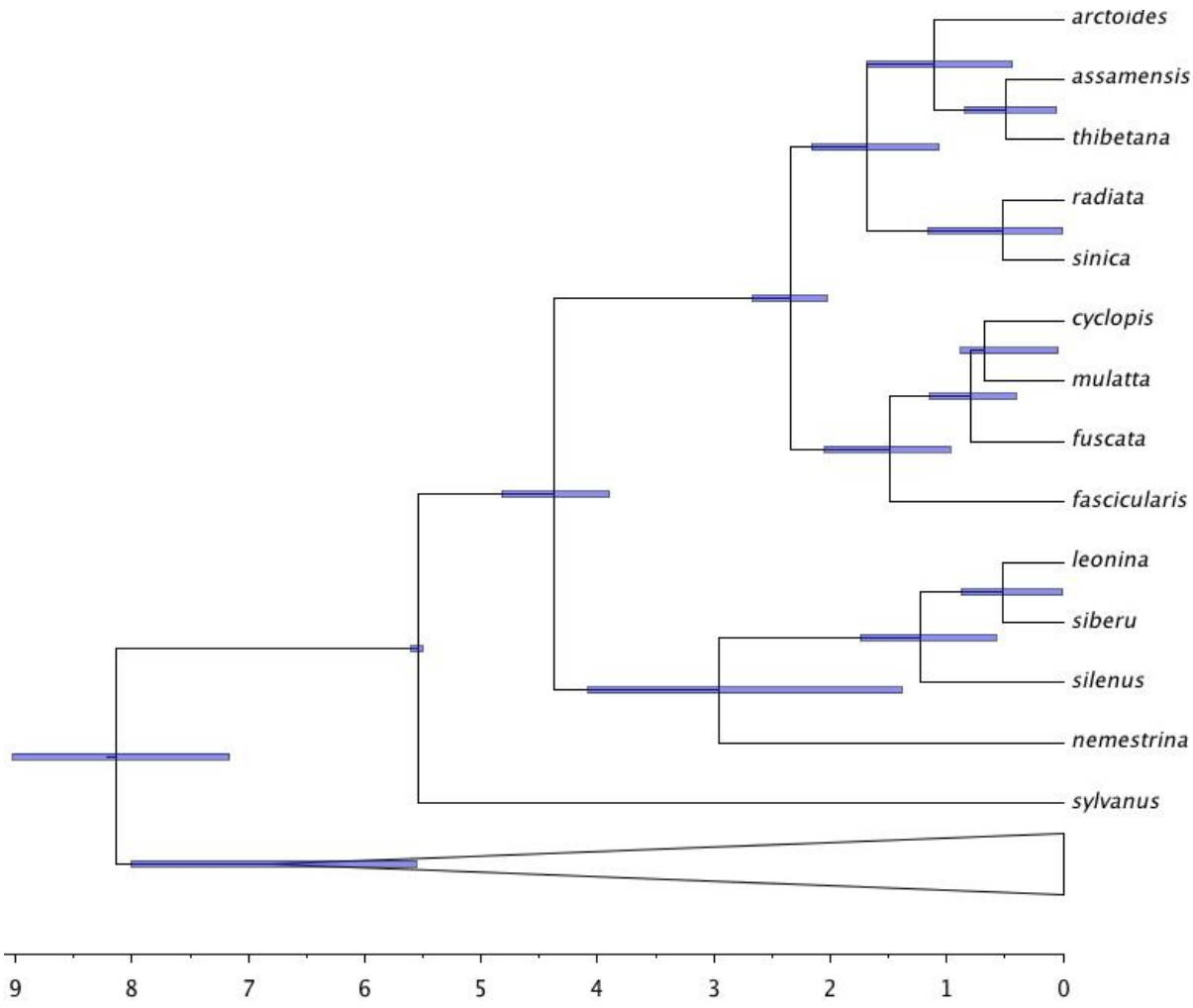

Figure S1. Most likely phylogenetic tree from the BEAST2 analysis for macaques and outgroup taxa using mtDNA and nuclear sequences. Blue horizontal bars represent the posterior 95% CI for the node ages.

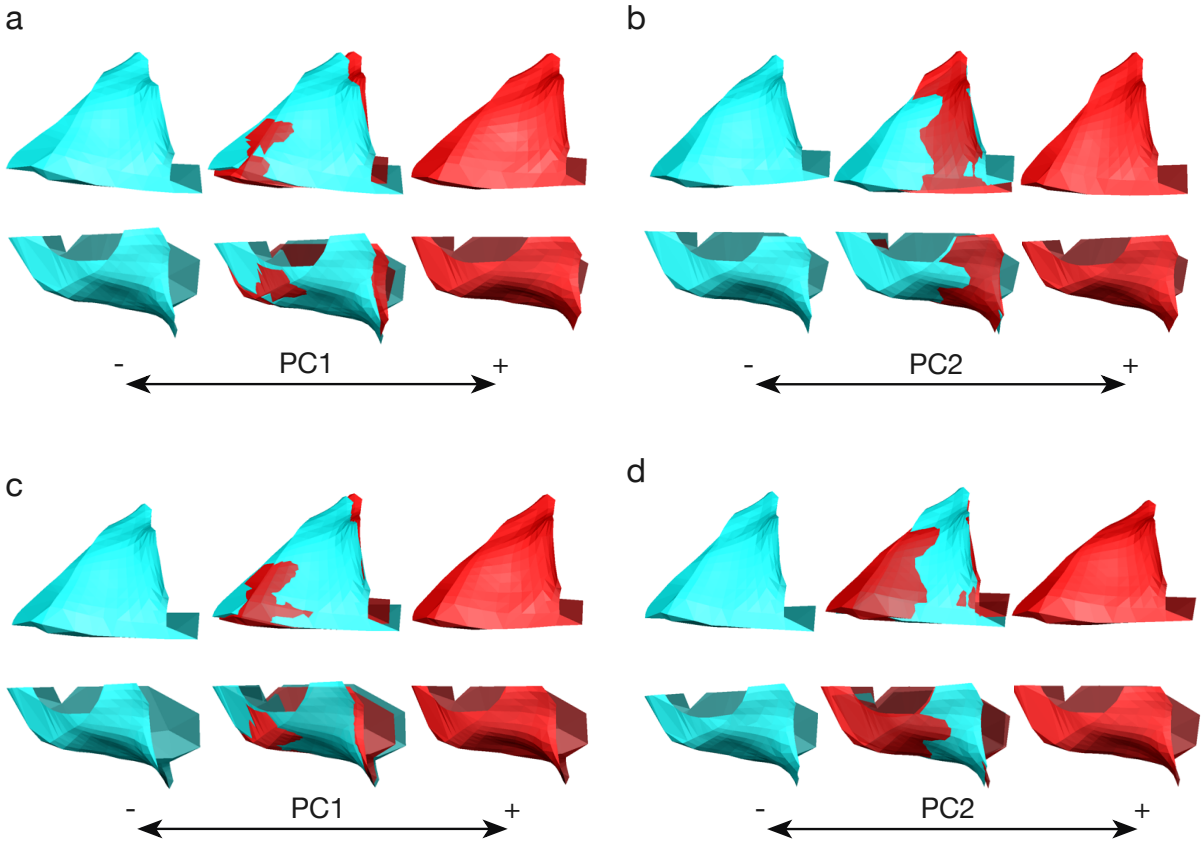

Figure S2. Shape changes along PC axes in the phylomorphospace. (a) PC1 and (b) PC2 based on the raw shape data. (c) PC1 and (d) PC2 based on the size-adjusted shape data. For more details, see the legend of Figure 6 in the main text.